Universitat Politècnica de València

Escola Tècnica Superior d'Enginyeria Agronòmica i del Medi Natural

Universitat Autònoma de Barcelona

Centre de Biotecnologia Animal i de Teràpia Gènica

Producción in vitro *de la proteína Klotho para el análisis de muestras humanas de cerebros de Alzheimer*

TRABAJO FIN DE GRADO EN BIOTECNOLOGÍA

Curso Académico: 2015-2016

ALUMNA: **Rebeca Blanch García**

TUTOR EXPERIMENTAL: **Miguel Chillon Rodríguez**

TUTORA UPV: **María José Bañuls Polo**

Valencia, septiembre de 2016

In vitro production of Klotho protein for analysis of Alzheimer's human brain samples

ABSTRACT

Klotho protein is a neuroprotective factor related to aging and Alzheimer's disease (AD). The secreted variant (s-KL) of the protein, which is the most expressed variant in humans, seems to have an important role in the maintenance of cognitive functions. Hence, the study of s-KL in humans is of high relevance for understanding its implications in AD and aging. In this work, the cDNA of the human s-KL protein was cloned in a eukaryote expression vector. s-KL protein was then produced by transient transfection in the HEK-293 human cell line, whose protein extracts were quantified and analysed by Western Blot. Immunodetection of s-KL was carried out through a specific antibody (K-18.2) never used before, for which a new protocol was developed as well. This assay allowed us to evaluate the production of s-KL by the transfected cells, as well as the specificity of the new K-18.2 antibody. Finally, a complementary validation of K-18.2 using protein extracts from human brains, obtained from both healthy and AD patients, was conducted.

Key Words

Klotho, Alzheimer's disease, cloning, transfection, Western blot, human, brain.

Producción in vitro de la proteína Klotho para el análisis de muestras humanas de cerebros de Alzheimer

RESUMEN

La proteína Klotho es un factor neuroprotector relacionado con el envejecimiento y la enfermedad de Alzheimer (AD, del inglés *Alzheimer's disease*). La variante secretada de la proteína (s-KL), que es la más expresada en humanos, parece tener un papel importante en el mantenimiento de las funciones cognitivas. Por ello, el estudio de la variante s-KL en humanos es de gran relevancia para poder entender su implicación en el AD y el envejecimiento. En este trabajo, el cDNA de la proteína s-KL humana fue clonado en un vector de expresión eucariota. Después, la proteína s-KL fue producida por transfección transitoria en la línea celular humana HEK-293, cuyos extractos proteicos fueron cuantificados y analizados por Western Blot. La inmunodetección de s-KL se llevó a cabo mediante un anticuerpo específico (K-18.2) nunca antes utilizado, y para el cual se desarrolló también un protocolo. Este ensayo permitió evaluar la producción de s-KL por las células transfectadas y la especificidad del nuevo anticuerpo K-18.2. Finalmente, se llevó a cabo una validación complementaria del anticuerpo K-18.2, utilizando extractos proteicos de cerebros humanos, obtenidos de pacientes sanos y enfermos de AD.

Palabras clave

Klotho, enfermedad de Alzheimer, clonaje, transfección, Western blot, humano, cerebro.

Producció in vitro de la proteïna Klotho per a l'anàlisi de mostres humanes de cervells d'Alzheimer

RESUM

La proteïna Klotho és un factor neuroprotector rel·lacionat amb l'envelliment i la malaltia d'Alzheimer (AD, de l'anglés *Alzheimer's disease*). La variant secretada de la proteïna (s-KL), la més expressada en humans, sembla tindre un paper important en el manteniment de les funcions cognitives. És per això que l'estudi de la variant s-KL en humans és de gran rellevància per poder entendre la seua implicació en l'AD i l'envelliment. En aquest treball, el cDNA de la proteïna s-KL humana va ser clonat en un vector d'expressió eucariota. Després, la proteïna s-KL fou produïda per transfecció transitòria en la línia cel·lular humana HEK-293, i els seus extractes proteics foren quantificats i analitzats per Western Blot. La immunodetecció de s-KL es va realitzar mitjançant un anticòs específic (K-18.2) mai abans utilitzat, i per al qual es va desenvolupar un nou protocol. Aquest assaig va permetre avaluar la producció de s-KL per les cèl·lules transfectades i la especificitat del nou anticòs K-18.2. Finalment, es va portar a terme una validació complementaria de l'anticòs K-18.2 utilitzant extractes proteics de cervells humans, obtinguts de pacients sans i malalts d'AD.

Paraules clau

Klotho, malaltia d'Alzheimer, clonatge, transfecció, Western blot, humà, cervell.

Autora: Rebeca Blanch García

Lugar de realización: Centre de Biotecnologia Animal i Teràpia Gènica (CBATEG) – Departament de Bioquimica i Biologia Mol·lecular (Universitat Autònoma de Barcelona).

Tutor experimental: Miguel Chillon Rodríguez

Tutora UPV: María José Bañuls Polo

Valencia, septiembre de 2016

AGRADECIMIENTOS

Como no podría ser de otra manera, quiero empezar agradeciendo a Miguel la oportunidad que me ha brindado de trabajar en su laboratorio. Gracias por tu confianza, por tu paciencia, por estar siempre dispuesto a resolver dudas y a ayudar en cualquier asunto más allá de nuestros experimentos. Gracias también a todos los compañeros de la 5ª planta, por hacerme el aterrizaje más fácil, por haberme enseñado tanto, y porque todos, en mayor o menor medida, habéis hecho posible que este trabajo saliera adelante. No ha sido fácil y ha habido momentos complicados, pero hoy puedo decir que de todo he aprendido, y que me siento satisfecha de poder presentar este Trabajo de Fin de Grado.

Sin embargo, para mí esto es más que un TFG; es la meta de un camino que empecé a recorrer hace años, y en el que me han acompañado muchas personas. Algunas siguen hoy a mi lado, aún a cientos de kilómetros. Otras ya no están tan *cerca*, pero siguen muy presentes. Porque sin ninguna de ellas habría sido lo mismo, porque su apoyo ha sido imprescindible. No hacen falta nombres, pero hay alguien que merece mención especial, porque ha estado presente de todas las formas posibles e imposibles en este camino. Porque su opinión fue decisiva hace cuatro años. Porque ha sido mi mentora extraoficial desde entonces, sin ninguna otra motivación que ganas de ayudar. Porque siguiendo sus pasos he llegado a este lugar tan lejos de casa, y ha sido todo un acierto. Porque es un ejemplo a seguir, como biotecnóloga, como investigadora, y sobre todo, como persona. Por todo esto, por hacérmelo más fácil, y por muchas otras cosas que tú ya sabes, gracias Irene. También quiero agradecerle a Helena su exhaustiva revisión, desde la otra parte del globo terráqueo, para evitar que mi atrevimiento con el inglés se convirtiera en *agresión* a la lengua de Shakespeare. Aunque digas que apenas te he dado trabajo, thank you very much.

Como tampoco podría ser de otra manera, quiero terminar agradeciendo a Carmen y Alberto todas las oportunidades que me han dado desde el día que nací. Porque nunca me han cerrado puertas y siempre me han dado alas. Porque me han apoyado en todos mis proyectos y, además, han hecho que fueran posibles. Si he llegado aquí, y de esta manera, es gracias a mis padres, y por ser como son, y por todo lo que han construido, me siento muy orgullosa de ellos.

Decía que este trabajo es una meta. Pero solo la primera. Porque este camino apenas lo acabo de comenzar y queda mucho por recorrer.

Y tengo muchas ganas de andar.

INDEX

FIGURE INDEX

TABLE INDEX

ABBREVIATIONS

Ab	antibody
Aβ	β-amyloid peptide
AD	Alzheimer's disease
ADAM	A Disintegrin And Metalloproteinase
Amp^R	Ampicillin resistance
APP	Amyloid precursor protein
Arg	Arginine
BCA	Bicinchoninic acid
bp	Base pairs
BSA	Bovine Serum Albumin
cDNA	Complementary DNA
CMV	Cytomegalovirus
CNS	Central nervous system
CSF	Cerebrospinal fluid
DMEM	Dulbecco's Modified Eagle's Medium
DNA	Desoxiribonucleic acid
dsDNA	Double stranded DNA
E.coli	*Escherichia coli*
EDTA	Ethylenediaminetetraacetic acid
FBS	Fetal Bovine Serum
FGF	Fibroblast growth factor
FOXO	Forkhead box O (transcription factor)
g	Gravity units
hAPP	Human amyloid precursor protein
HEK-293	Human Embryonic Kidney 293 cell line
hKLS	Human secreted Klotho protein (human s-KL)

HRP	Enzyme horseradish peroxidase
IFNγ	Interferon gamma
IGF-1	Insulin-like growth factor 1
IGF-1R	IGF-1 Receptor
IRS	Insulin receptor substrate
Kan^{R}	Kanamycin resistance
Kb	Kilobase (1000 DNA base pairs)
kDa	Kilo Dalton (Protein molecular weight units)
kHz	Kilohertz (Frequency units)
KL	Klotho protein
kl-/kl-	Klotho-deficient mice
Lys	Lysine
m-KL	Transmembrane Klotho protein
mKLS	Murine secreted Klotho protein (murine s-KL)
mM	Milimolar
MnSOD	Manganese superoxide dismutase
mRNA	Messenger RNA
NFTs	NFTs neurofibrillary tangles
PEI	Polyethylenimine
PHF	Paired helical filaments
Pi	Phosphate
p- KL	Cleaved or processed Klotho protein
PSEN1	Presenilin-1
PSEN2	Presenilin-2
PTH	Parathyroid hormone
ROS	Reactive oxygen species
rpm	Revolutions per minute

sAPPα	soluble form of APP
SDS	Sodium dodecyl sulphate
SDS-PAGE	SDS-Polyacrylamide gel electrophoresis
SF	Straight filaments
s-KL	**s**ecreted form of Klotho protein
TEMED	Terametil-etilen-diamina
TNFα	tumor necrosis factor alpha
Tris	Tris(hydroxymethyl)aminomethane
TRPC-1	Transient receptor potential channel 1
TRPV	Transient receptor potential cation channel subfamily V
U	Units of restriction enzyme
UV	Ultraviolet light
VEGFR2	Vascular endothelial growth factor receptor-2
1,25(OH)2D3	1-alpha,25-dihidroxicolecalciferol or calcitriol or D vitamin.
3xTg-AD mice	Triple transgenic mouse model of Alzheimer's disease

1. INTRODUCTION

1.1. Alzheimer's disease

Alzheimer's disease (AD) is one of the most common neurodegenerative diseases, involving the progressive loss of mental, behavioural, functional decline and ability to learn (Anand, Gill, & Mahdi, 2014). AD accounts for more than 80% of dementia cases, and has become a leading cause of death and disability in aged people worldwide (Kumar, Singh, & Ekavali, 2015). One person for every 85 individuals can be expected to suffer from AD by the year 2050 (Brookmeyer, Johnson, Ziegler-Graham, & Arrighi, 2007). However, the pathogenesis of AD is not yet fully understood (Kuang et al., 2014).

Etiology of AD is multifactorial with genetic, environmental, behavioural and developmental components playing role (Anand et al., 2014). Several hypotheses have been proposed to explain the pathophysiology of AD. They include:

- Aberrant β-amyloid (Aβ) metabolism, giving rise to Aβ extracellular plaques.
- Hyperphosphorylation of cytoskeletal proteins like tau, causing intraneuronal deposits.
- Mutations in genes coding for presenilin-1 and -2 (PSEN1 and PSEN2, respectively) and amyloid precursor protein (APP).
- Apolipoprotein E genotype.
- Oxidative stress.
- Excitotoxicity.
- Inflammation.
- Abnormal cell cycle re-entry.

However, none of these hypotheses alone is sufficient to explain the different biochemical and pathological abnormalities in AD (Kumar & Dogra, 2008). Despite the diversity of the mechanisms involved, neuronal death is the inevitable event resulting in AD (Anand et al., 2014).

It is commonly accepted that the causes leading up to memory decline are strongly tied to deposits of misfolded protein aggregates (Ross & Poirier, 2004). Beta-amyloid (Aβ) plaques and neurofibrillary tangles (NFTs) are the hallmark deposits in AD brains (Lewczuk, Mroczko, Fagan, & Kornhuber, 2015) (**Figure 1**). These aggregates derive from the naturally occurring and crucial protein structures in the brain Aβ and tau (Muresan & Ladescu Muresan, 2015; Nhan, Chiang, & Koo, 2015). However, their abnormal aggregation causes progressive neuronal death, memory impairment, and cognitive disturbances (Tanzi & Bertram, 2005).

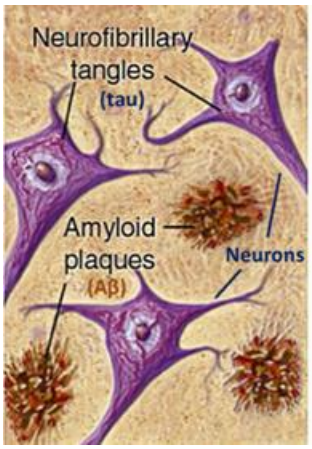

***Figure 1*. Protein aggregates in an Alzheimer's diseased brain.**
Neurofibrillary tangles of tau and amyloid plaques of Aβ accumulate inside neurons and in the extracellular space, respectively. Adapted from *BrightFocus Foundation* (2016). Retrieved September 2016 from http://www.brightfocus.org/alzheimers/infographic/amyloid-plaques-and-neurofibrillary-tangles.

1.1.1. Protein deposits behind AD: Aβ and tau

Aβ plaques

Recent studies highlight the role of Aβ oligomers in synaptic impairment, suggesting that these are primarily the only one among several other signals that destroy the integrity of brain functions (Anand et al., 2014).

Aβ derive from the amyloid precursor protein (APP), which is a type I membrane glycoprotein having multiple isoforms generated by alternative splicing. However, physiological functions of APP are poorly understood (Müller & Zheng, 2012). There are two proteolytic processing pathways of APP, as shown in **Figure 2**. In the non-amyloidogenic pathway, APP is cleaved by α-secretases, resulting in the production of the soluble form of APP (sAPPα), which has several neuroprotective properties. In the amyloidogenic pathway, APP is aberrantly processed by β-secretases, generating a membrane-bound C-terminal fragment (C99), which is subsequently cleaved by γ-secretases. As a result, the Aβ peptide is generated (Nunan & Small, 2000), causing an imbalance between production and clearance of Aβ peptide (Salomone, Caraci, Leggio, Fedotova, & Drago, 2012). As a consequence, Aβ peptides spontaneously aggregate into soluble oligomers and join each other to form insoluble fibrils of beta-sheet conformation, which are eventually deposited in diffuse senile plaques (Hardy, 2009). It has been observed that Aβ oligomers induce oxidative damage, promote tau hyperphosphorylation, and result in toxic effects on synapses and mitochondria (Kumar & Dogra, 2008). In short, Aβ oligomers aggregates are considered to be responsible for the neuronal and vascular degeneration in AD brains (Roth, Ramírez, Alarcón, & Von Bernhardi, 2005).

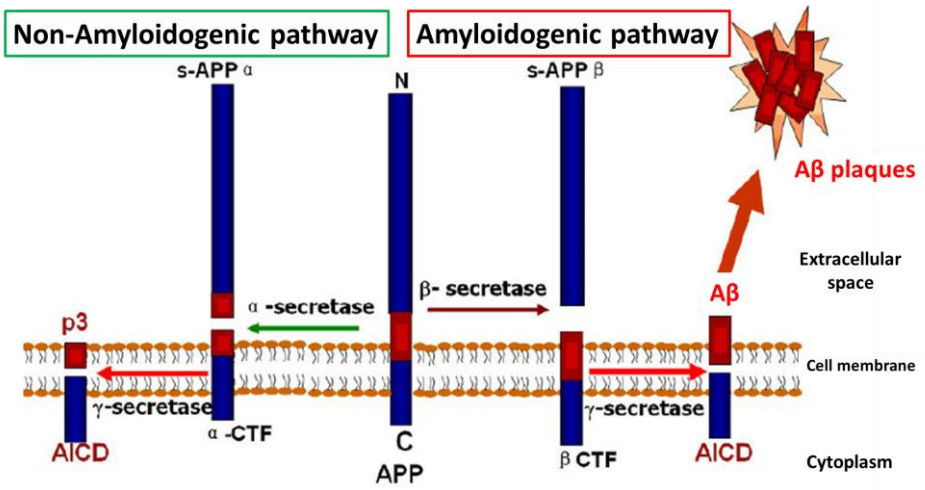

Figure 2. **Proteolytic processing pathways of APP**: non-amiloidogenic (left) or amyloidogenic (right).

Hyperphosphorylated tau

Tau proteins are mainly found in neurons and belong to the family of microtubule-associated proteins (Tucker, 1990). Six isoforms of tau proteins identified in the adult brain play an important role in microtubule assembly and stabilization of neuronal microtubules network (Lee, Neve, & Kosik, 1989). The phosphorylation of tau protein is developmentally regulated from foetal to adult stage (Butler & Shelanski, 1986). However, when abnormally hyperphosphorylated, tau has a reduced affinity towards microtubules (Mazanetz & Fischer, 2007). The hyperphosphorylated tau proteins polymerized into paired helical filaments (PHF)

and straight filaments (SF) are referred to as neurofibrillary tangles (NFTs) (Köpke et al., 1993). The loss of normal tau function leads to a pathological disturbance in structural and regulatory functions of the cytoskeleton, which affect normal cellular functions of neurons, for instance the maintenance of appropriate morphology and the axonal transport, causing synaptic dysfunction and neurodegeneration (Roy, Zhang, Lee, & Trojanowski, 2005).

1.1.2. AD treatments and its major risk factor, age

The multiplicity of mechanisms involved in the pathogenesis of AD make difficult to develop an effective treatment for AD (Anand et al., 2014). To date, approved drugs just slow disease progression, reduce problematic behaviours or alleviate cognitive symptoms, but do not alter the course of the disease. In addition, these therapies only show efficacy in a reduced number of patients, for a short period of time, and undesirable side effects are frequently observed. Thus, further research is needed to fully understand Alzheimer's etiology, improve its early diagnosis and develop effective drugs capable of block or completely cure the disease.

The major risk factor for AD is age, with a sharp increase in incidence after 60 years (Kawas et al., 2000). This is why many researchers agree that in order to understand AD, we must understand its inherent relationship to aging (Herrup, 2010). With the growing longevity of population in the last decades, AD prevalence has highly increased, and it is already reaching epidemic proportions with no cure or preventive therapy yet available (Tanzi & Bertram, 2005).

The progressive loss of both cognitive functions and the ability to form new memories that occurs associated to neurodegenerative diseases like AD is known as *dementia*, and it must not be understood as the memory loss associated to aging, in which the intellectual and behavioural functions of the person work correctly. In other words, dementia is not a part of the normal process of aging, but is considered a pathology, being AD the most important type. However, both pathological and non-pathological processes could be associated to common factors, for instance the IGF-1 pathway, in which the Klotho (KL) protein is involved. This protein has been associated with the maintenance of cognitive functions, so it has become a promising research line to better understand the neurodegeneration related to both AD and non-pathological aging.

1.2. Klotho

The **Klotho gene**, named after the Greek goddess who spins the thread of life, **was discovered** in 1997, when its mutation caused systemic aging and shortened longevity in mice (Kuro-o et al., 1997). The aging phenotypes included impaired cognition, arteriosclerosis, decreased bone mineral density, and sarcopenia (Kuro-O, 2010). Conversely, overexpression of *klotho* extended the life span in mice (Kurosu et al., 2005), which supports the perception of *klotho* as an aging-suppressor gene.

The expression of *klotho* is specific to certain tissues including kidney, brain and the parathyroid gland. In the brain, *klotho* is highly expressed in the ependymal cells of the choroid plexus and in Purkinje EC cells, as well as in hippocampal neurons (Kuro-o et al., 1997). Recently, both Klotho mRNA and protein were detected throughout the brain parenchyma, co-localizing in neurons and oligodendrocytes during early postnatal development (Clinton et al., 2013). This suggests that Klotho protein may influence a variety of structures and functions during the central nervous system (CNS) maturation and aging.

Klotho-deficient mice (kl-/kl-) have fewer dopaminergic neurons (Kosakai et al., 2011), neuronal degeneration in the hippocampus (Shiozaki et al., 2008), hypomyelination (Chen et al., 2013),

fewer synapses and lower synapse-related protein levels compared to wild-type mice (Li et al., 2004; Shiozaki et al., 2008). In addition, they show deficient axonal transport (Uchida et al., 2001). Behavioral studies also indicate that kl-/kl- mice have deficits in memory retention (Nagai et al., 2003), probably due to an increase in the oxidative stress in the brain.

In contrast, **mice overexpressing *klotho*** perform better in Morris Water-Maze tests (Nagai et al., 2003), which evaluate hippocampus-dependent spatial memory and learning. In other studies, it was observed that overexpression of *klotho* extends life by attenuating generation of reactive oxygen species evoked by insulin and IGF-1 signaling (Kurosu et al., 2005; Yamamoto et al., 2005). Wnt, TNFα and IFNγ signaling are augmented in Klotho-deficient mice, which contribute to accelerated aging (Liu et al., 2007).

Apart from that, recent studies in humans cohorts showed that carriers of the Klotho *KL-VS* allele, which increases secretion of Klotho *in vitro*, obtained better results in various cognitive tests, including verbal capacity, executive function, visual-spatial processing, and learning (Dubal et al., 2014). A meta-analysis of the *KL-VS* variant indicated that it is associated with healthy aging (Di Bona, Accardi, Virruso, Candore, & Caruso, 2014).

1.2.1. Klotho gene and protein structure

In mice and humans, the *klotho* gene is composed of five exons and encodes a transcript of 5.2 kb. In the third exon, there is an alternative splicing donor site that can generate two different transcripts (Matsumura et al., 1998; Shiraki-Iida et al., 1998).

The full-length transcript encodes a single pass transmembrane protein (1014 and 1012 amino acids in mouse and human, respectively) with a molecular weight of approximately 130kDa (**m-KL**). The intracellular domain is very short (~10 amino acids), and it does not have functional domains. The extracellular domain has two internal repeats, KL1 and KL2, linked by a region containing four basic amino acids (Lys-Lys-Arg-Lys) that form a potential site for proteolytic cleavage (Kim, Hwang, Park, Kong, & Cha, 2015). Membrane proteases such as ADAM10 and ADAM17 (ADAM metalloproteinase domain 10 and 17, respectively) cleave the extracellular domain of Klotho in this site, generating the so called *cleaved* or *processed* Klotho **(p-KL)**, which is released into blood, urine and cerebrospinal fluid (Bloch et al., 2009), and functions as an endocrine, autocrine and paracrine hormone on target cells (Kuro-o et al., 1997; Kurosu et al., 2005).

The transcript generated by alternative splicing is composed of 3 exons in mouse and 5 exons in human. It encodes the secreted form of the protein (**s-KL**), also called *truncated transcript*, which is formed solely by the KL1 domain (composed of 549 and 550 amino acids in mouse and human, respectively), with an approximate weight of 70kDa. This secreted form of the protein contains an exclusive peptide tail at C-terminus (15 amino acids for murine s-KL, and 16 amino acids for human s-KL), which is not present in the transmembrane nor in the processed forms (Xu & Sun, 2015).

In mice, the transmembrane form of *klotho* transcript (*m-KL*) predominates over the secreted form (*s-KL*), while in humans, the *s-KL* is the most expressed.

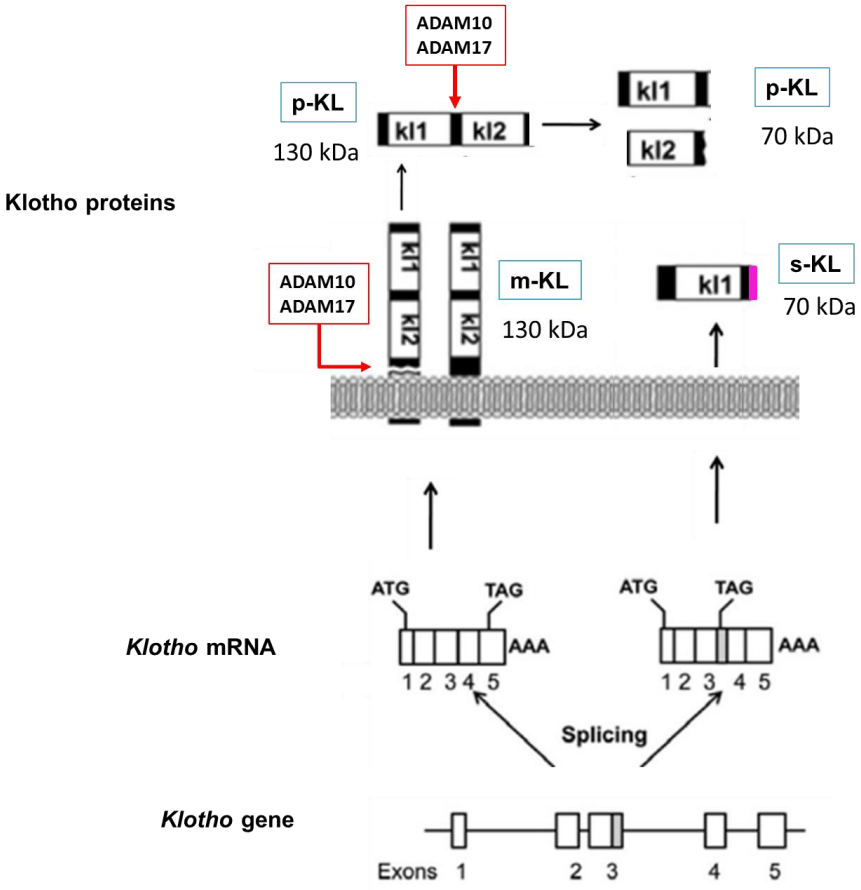

***Figure 3*. Schematic structures of Klotho gene, mRNA and protein variants.** The resultant alternatively spliced transcript contains 50bp insertion after exon 3, represented in grey. The exclusive peptide tail at C-terminus of s-KL is marked in purple. Extracellular domain of membrane Klotho (m-KL) containing KL1 and KL2 repeats is cleaved by α- and β-secretases (ADAM10 and ADAM17), represented in red. Adapted from *Hu, Kuro-o, & Moe, 2012*.

1.2.2. Molecular functions of Klotho

Processed (p-KL) and secreted Klotho (s-KL) are referred to as **soluble klotho**, as they are both released into body fluids - blood, urine and cerebrospinal fluid (CSF) - being s-KL the major form of soluble Klotho. However, no previous studies have evaluated the particular properties of each soluble variant separately. This is due to the fact that, to date, all the commercial antibodies are directed to the common domain KL1, so they are not capable to discriminate between p-KL and s-KL. Hence, the discovered functions of the soluble Klotho have been attributed to both variants.

Soluble Klotho works as a humoral factor that targets multiple tissues and organs. It exerts pleiotropic activities including regulation of oxidative stress, growth factor signaling, and ion homeostasis. In addition, soluble Klotho is involved in organ protection and has anti-aging effects. Soluble Klotho has direct effects on tissues and cells that do not express Klotho, which partially explains why a mutation in the *klotho* gene causes such extensive aging phenotypes. Therefore, Klotho may function as a hormone, although the binding sites or the receptors for Klotho remain unknown (Xu & Sun, 2015). Hence, it would be important to identify and characterize Klotho receptors and investigate its downstream signaling in future studies. Apart from this, it was reported that circulating levels of soluble Klotho decrease with age, and the *klotho* gene is associated with increased risk of age-related diseases (Kim et al., 2015).

Below, we summarize the main molecular functions in which the transmembrane and the soluble forms of Klotho seem to be implicated.

1.2.2.1. Inhibition of the insulin/IGF-1 signaling pathway

Several studies have reported that disruption of Klotho expression decreases insulin production and increases insulin sensitivity (Utsugi et al., 2000). Klotho knockout mice also exhibit less energy storage and less energy expenditure compared with wild-type mice (Mori et al., 2000). Several studies have shown that Klotho suppresses the downstream signaling pathway of the insulin receptor substrate (IRS) and the IGF-1 receptor (IGF-1R) without directly binding to these receptors (Kurosu et al., 2005). Therefore, Klotho may indirectly regulate the insulin/IGF signaling pathway (Wang & Sun, 2009), although the exact mechanism remains to be elucidated.

1.2.2.2. Suppression of WNT signaling

It was reported that Klotho binds to different types of Wnt ligands to suppress the downstream signaling transduction, and also that Klotho knockout increases Wnt signaling in mice (Liu et al., 2007). The activated Wnt3 signaling pathway prolongs the cell cycle by arresting it at the G_2/M phase and up-regulating fibrogenic cytokines. Conversely, the Klotho treated cells bypass this phase and exhibit reduced fibrogenic cytokines production (Satoh et al., 2012). Hence, Klotho may suppresses the Wnt signaling, so it could also possess anti-cancer and antioxidative properties.

1.2.2.3. Participation in Ca^{2+} homeostasis

Soluble Klotho increases the abundance of cation channel TRPV5 on the cell membrane (Chang et al., 2005). In HEK-293 cells that are co-transfected with *TRPV5* and *klotho*, calcium (Ca^{2+}) uptake is increased in proportion to *klotho* expression (Asai et al., 2012). In a transgenic mouse model with targeted disruption of the *klotho* gene in the renal distal tubule, a decrease in TRPV5 expression in the distal tubular cells was accompanied by a mild increase in urinary calcium excretion (Olauson et al., 2012). Klotho may therefore regulate calcium metabolism via TRPV5. Nevertheless, no significant association between Klotho and TRPV5 expression has been found in the kidney yet. Some reports indicate that Klotho binds to vascular endothelial growth factor receptor-2 (VEGFR2) and transient-receptor potential canonical Ca^{2+} channel 1 (TRPC-1) through its KL2 domain, and regulates TRPC-1-mediated Ca^{2+} flux entry to maintain endothelial integrity (Kusaba et al., 2010). A recent study indicated that Klotho increases the plasma membrane retention of TRPV2, leading to enhanced glucose-induced insulin secretion in pancreatic β-cells (Lin & Sun, 2012). It will be of interest in future studies to assess how soluble Klotho regulates multiple ion channels and how the ion flux contributes to the aging process.

1.2.2.4. Participation in phosphate homeostasis and vitamin D metabolism

Phosphate (Pi) is essential to a variety of physiological processes and is regulated by D vitamin (1,25(OH)2D3), the parathyroid hormone (PTH), and fibroblast growth factor 23 (FGF23) (Tanaka & Deluca, 1974). Pi absorption increases the secretion of FGF23, a bone-derived hormone that is critical in the regulation of the renal excretion of Pi (Farrow, Imel, & White, 2011). Secreted FGF23 has a low affinity to its receptors (FGFRs). Transmembrane Klotho binds to FGFRs to enhance the binding ability of FGF23. This binding activates a MAPK cascade, which inhibits Pi reabsorption in renal proximal tubule cells and suppresses the

expression Cyp27b1 gene that encodes 1-α-hydroxylase, which hydrolyzes 25-dihydroxyvitamin D3 to generate 1,25(OH)2D3 (Kuro-o, 2006; Urakawa et al., 2006).

1.2.2.5. Suppression of oxidative stress

FOXO3a up-regulates the expression of manganese superoxide dismutase (MnSOD), an important enzyme for mitochondrial antioxidant defences in mammalian cells (Kurosu et al., 2005; Yamamoto et al., 2005). FOXO3a functions as a negative regulator of mitochondrial reactive oxygen species (ROS) generation. Klotho increases FOXO3a phosphorylation, suggesting that Klotho may suppress ROS-related oxidative stress. *Klotho* overexpression decreases H_2O_2-induced apoptosis, β-galactosidase activity, mitochondrial DNA fragmentation, superoxide anion generation, lipid peroxidation, and Bax protein expression (Wang, Kuro-O, & Sun, 2012). Although the mechanism by which Klotho extends the cellular life span is not fully understood, a recent study indicates that low levels of ROS-related stress responses are beneficial to the organism and can extend the life span of a cell (Sena & Chandel, 2012). This result suggests that the anti-aging function of Klotho may involve ROS and its downstream signaling pathways.

In conclusion, the discovered functions of Klotho point out that this protein plays an important role in neurodegenerative and age-related diseases.

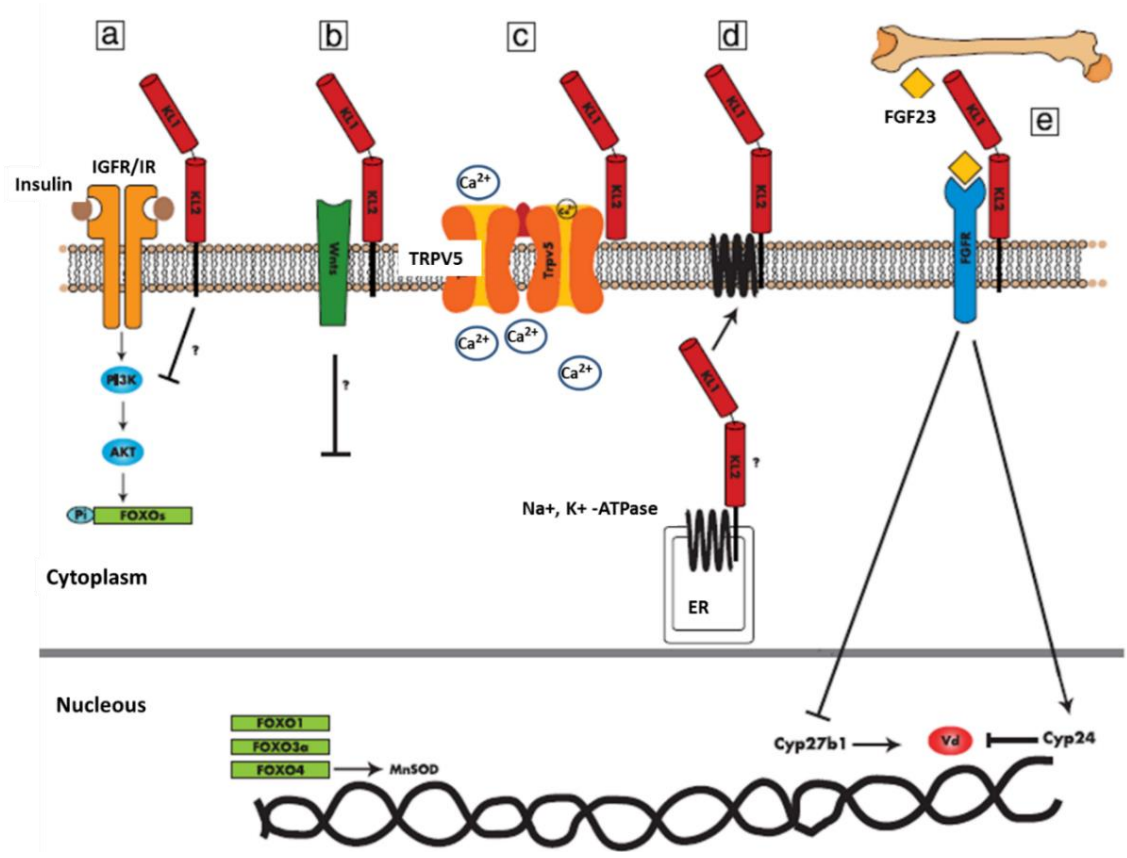

***Figure 4*. Overview of the functions of Klotho.** (a) Klotho inhibits the IGF signaling pathway. The downstream factors FOXO1, -3a, and -4 mediate the function of Klotho. (b) Klotho suppresses the Wnt signaling pathway. (c) Klotho regulates TRPV5 calcium channels. (d) Klotho regulates PTH synthesis. (e) The Klotho-FGF23 complex regulates Pi absorption, mineral metabolism, and vitamin D_3 expression and activity. Adapted from Xu & Sun, 2015.

1.3. Previous studies relating Klotho, AD and aging

Klotho is a neuroprotective factor, as demonstrated *in vitro* on hippocampal neurons against glutamate and beta-amyloid peptide (Aβ) cytotoxicity through an increased resistance to oxidative stress (Zeldich et al., 2014). Klotho was also able to counteract cognitive deficits and premature mortality in human amyloid precursor protein (hAPP) transgenic mice J20, a well-characterized animal model of Alzheimer's disease (Dubal et al., 2015). In addition, Klotho is a synaptic modulator that increases the expression of acetylcholine transferase, whose continued activity diminution has been correlated with an increase in cognitive deficits ((Bohnen et al., 2005).

It was suggested that Klotho might prevent the development of AD associated with aging, probably by inhibiting insulin/IGF-1 signaling and consequently the oxidative injury in the brain. However, no previous studies had directly connected Klotho and the AD phenotype until 2014, when Semba *et al.* analyzed Klotho in the CSF of older adults with Alzheimer's disease and in older and younger adults with normal cognition. They concluded that Klotho concentrations in the CSF were significantly lower in older adults with Alzheimer's disease compared to older adults with normal cognition. They also reported that Klotho levels were lower in CSF of older adults compared to younger adults (Semba et al., 2014). Even though this study revealed a connection between diminished levels of soluble Klotho and AD and aging, it did not specify whether these variations correspond to the processed (p-KL) or to the secreted (s-KL) form of the protein. This is due to the fact that, thus far, all the commercial antibodies available recognize an epitope located in the KL1 domain, which is common in all Klotho forms, as previously explained. Thus, the antibodies used were not able to discriminate s-KL from the KL1 domain cleaved from the transmembrane isoform (p-KL).

In order to overcome this limitation, our group generated a new antibody (Ab-K113) against the exclusive peptide tail at the C-terminus of the s-KL protein in mice. This antibody was used to detect s-KL in different brain areas of young (6-month-old) and old adult mice (18-month-old). They observed that the levels of s-KL protein declined with aging in all brain areas analyzed, but in the cerebellum, in which s-KL levels were similar at both ages. It should be noted that this was the first time that the levels of the alternatively spliced secreted Klotho protein (s-KL) were specifically quantified without interference from the KL1 or KL1+KL2 domains produced after cleavage of the transmembrane Klotho protein (Massó et al., 2015).

Apart from that, our team analyzed the expression profiles of both transmembrane (m-KL) and secreted (s-KL) *Klotho* in kidney and brain, the organs in which it is more expressed. It turned out that expression levels of the two *Klotho* transcripts decayed with age in both organs. It was also observed that in mouse kidney, the expression of *m-KL* was higher than that of *s-KL*, as previously described by other groups (Bektas et al., 2004). Likewise, the expression of *m-KL* in the brain was also higher than that of *s-KL*.

Given the structural and functional heterogeneity of the brain, our team studied whether the reduced expression of *klotho* associated with aging was uniform throughout this organ or was more pronounced in some areas than in others. They observed that in all the brain areas analyzed, the expression of both *klotho* transcripts decayed with aging. Moreover, this decay was not uniform throughout the brain, and the decay of *s-KL* had a different profile to that of *m-KL*. This suggested a different regulation of their expression, and/or possible different roles for *s-KL* and *m-KL* protein variants.

Apart from this, our group analyzed whether the reduction observed in the expression of the *s-KL* and *m-KL* transcripts in the different brain areas during non-pathological aging was also observed

in pathological aging, as happens in neurodegenerative disorders like Alzheimer's disease. They analyzed the expression profile of the *s-KL* and *m-KL* transcripts in different brain areas of 6-, 9-, and 12-month-old 3xTg-AD mice, a suitable animal model for Alzheimer's disease. As observed in non-pathological aging, the expression of both transcripts declined rapidly, but in the 3xTg-AD transgenic model of Alzheimer's disease, *klotho* decayed more rapidly compared to healthy animals of the same age. However, during aging, differences in the expression profile of *s-KL* and *m-KL* were reduced, and at 12 months of age, *s-KL* and *m-KL* levels were similar in 3xTg-AD and control mice.

As observed for *s-KL* mRNA expression, levels of the s-KL protein were also lower in 3xTg-AD mice. Thus, compared with healthy aged-matched controls, s-KL protein levels were reduced at 6 and 12 months of age. In other words, s-KL levels in 3xTg-AD mice were low even before symptoms like amyloidogenic plaques appeared, what enhances its potential as an early biomarker of AD.

In short, the research of Massó *et al.* showed for the first time that the *klotho* transcript produced by alternative splicing generates a stable protein (s-KL) of 70kDa, and that in contrast to the transmembrane Klotho isoform (m-KL), it is ten times more abundant in the brain than in the kidney. They also demonstrated that s-KL and m-KL have different expression profiles and localization, suggesting that the different forms of Klotho protein have different regulation of their expression, and/or possible different roles.

Given that s-KL is highly expressed in brain and it has a neuroprotective role, it seems that s-KL has a crucial role in key areas for cognitive function, which are targets of study in both aging and neurodegenerative diseases. This, together with the fact that the s-KL isoform is the most expressed in humans (Shiraki-Iida et al., 1998) - in contrast to mice, in which the m-KL is more abundant -, could indicate that the s-KL isoform is even more relevant in humans.

Thus, we focused our research in the human s-KL protein variant in order to elucidate the way in which its deficiency leads to the decline of cognitive functions associated to aging and Alzheimer's disease. To this end, our group generated a new antibody (K-18.2) specific for the human form of s-KL, since its exclusive tail is not homologue to that of the murine s-KL, for which the K113 antibody had previously been produced and was available at our laboratory.

2. OBJECTIVES AND WORKFLOW

The aim of this work is to clone the cDNA of the human secreted form of Klotho protein (human s-KL, hereafter named hKLS) into a eukaryote expression vector, and to transfect it into the human cell line HEK-293. The *in vitro* produced hKLS protein would be used for two different and complementary approaches:

- On the one hand, to validate the new K-18.2 antibody, specifically designed by our group to detect the hKLS protein.
- On the other hand, to build a calibration curve which allows the relative quantification of hKLS in human samples.

Having these tools optimized, the future goal will be to analyse the hKLS protein in human samples of healthy and AD patients, and to correlate its levels with the progression and severity of the disease.

Workflow:

1. Amplification of the hKLS cDNA

1.1. Transformation of competent *E.coli* bacteria using the synthetic pEX+hKLS plasmid.
1.2. Pre-culture of transformed colony.
1.3. DNA minipreparation of the pre-cultured colony.
1.4. Verification of the transformation by enzymatic DNA digestion.
1.5. DNA maxipreparation of the transformed colony.

2. Cloning the hKLS cDNA into an eukaryote expression vector (pGV)

2.1. Enzymatic digestions of pEX-hKLS amplified plasmid and the pGV acceptor vector.
2.2. Separation of DNA fragments by electrophoresis in agarose gel.
2.3. Purification of the hKLS insert and the linealized pGV vector from gel.
2.4. Dephosphorilation of the linealized pGV ends.
2.5. DNA quantification.
2.6. Ligation of the hKLS insert to the pGV vector.

3. Verification of the ligation

3.1. Transformation of competent *E.coli* bacteria using the expression vector pGV+hKLS.
3.2. Selection and pre-culture of transformed bacteria.
3.3. DNA minipreparations.
3.4. Verification of the ligation by enzymatic DNA digestions and electrophoresis.
3.5. Amplification of the positive ligation by maxipreparation.
3.6. DNA quantification.
3.7. Verification of the amplified colony by enzymatic DNA digestions and electrophoresis.

4. In vitro production of the hKLS protein

4.1. Transfection of HEK-293 cells using the pGV+hKLS expression vector.
4.2. Protein extraction.
4.3. Protein quantification by spectrophotometry.

5. hKLS protein analysis by Western Blot

5.1. Optimization of K-18.2 antibody protocol using protein extracts from mice.
5.2. Denaturing protein electrophoresis (SDS-PAGE).
5.3. Electrotransference.
5.4. Immunodetection of hKLS using the K-18.2 antibody.

3. MATERIALS and METHODS

3.1. Bacterial strains

Chemically competent bacteria were produced in our laboratory using *E.coli* TOP10^{R} (Invitrogen) strain. Competent bacteria are able to incorporate exogenous DNA, and were used to amplify plasmidic DNA smaller than 10kb.

3.2. In vitro cell lines

Human embryonic kidney cell line, HEK-293 QB (ATCC® CRL-573^{TM}, Q-BIOgene) was propagated in Dulbecco's Modified Eagle's Medium (DMEM) (PAA laboratories) supplemented with 10% v/v Fetal Bovine Serum (FBS) (PAA laboratories) and Penicillin (100 I.U/ml)/Streptomycin (100 I.U/ml) (PAA Laboratories) at 37ºC and 5% CO_2.

3.3.DNA constructs

pEX+hKLS plasmid

The gene coding the human secreted Klotho protein (hKLS) was designed by our group and ordered to Eurofins Genomics (Ebersberg, Germany) in the pEX-K4 plasmid (Kan^{R}).

pGV vector

The kKLS gene was cloned in the mammalian expression vector pGV (Amp^{R}) under the control of the cytomegalovirus (CMV) promoter, obtaining de pGV+hKLS construct. This plasmidic pGV vector was generated in our laboratory.

pDsRed2-Mito Vector

pDsRed2-Mito (Conda), designed for fluorescent labeling of mitochondria, is highly expressed in mammalian cells. It encodes a fusion of *Discosoma sp.* red fluorescent protein (DsRed2) and a mitochondrial targeting sequence of human cytochrome c oxidase subunit VIII (Mito). pDsRed2-Mito Vector (Amp^{R}) was used as a positive control in the transfection experiments.

3.4. Murine samples

Murine brain samples were obtained from 12 month old, C57Bl6 male mice (Harlan Laboratories BV), which exhibit a wild type phenotype.

3.5. Human samples

Human brain samples were provided by Dr. Isidre Ferrer, from the biobanc of the Hospital del Bellvitge. Brain samples were obtained from deceased donors, both healthy and AD patients and kept at -80ºC.

3.6. Stock solutions

The composition of the solutions and buffers prepared in our laboratory and used in the protocols is detailed below:

DNA minipreparations

- **P1** or **Resuspension buffer** (4ºC): 50mM Tris-HCl (Sigma) pH=8.0, 10mM EDTA (USB), 100mg/mL RNasaA (QIAGEN).

- **P2** or **Lysis buffer** (RT): 200mM NaOH (Panreac), 1% (w/v) SDS (Amresco).
- **P3** or **protein precipitation buffer** (4ºC, pH=5.5): 3M AcK (Sigma).

DNA agarose gel electrophoresis

- **Loding buffer**: 50% glicerol (v/v) (Sigma-Aldrich), 100mM EDTA pH 8.0 (USB), 1% SDS (p/v) (Iberlabo), 0.1% (p/v) bromofenol blue or Xylene Cyanol FF.
  Bromophenol blue and Xylene Cyanol FF run toward the anode as 500bp and 4kb bands, respectively. The choice of one of them depends on the DNA fragment size we expect to separate.
- **TAE 1x** (pH=8.0): 40mM Tris-acetic, 0.1mM EDTA.

Transfection of cultured cells

- **PBS (phosphate buffered saline)** (pH= 7.4): 137mM NaCl (Panreac), 3mM KCl (Panreac), 10mM Sodium Dihydrogen Phosphate Dodecahydrate (Panreac), 1.7mM Potassium dihydrogen phosphate (Panreac).

Protein extraction

- **RIPA buffer:** 50mM Tris-HCl pH 7.4 (Sigma), 150mM NaCl (Panreac), 1mM EDTA (USB), 1% (v/v) NP-40 (Fluka), 0.25% (v/v) Sodium Deoxycholate (Sigma), 50mM Sodium fluoride (Sigma), 1mM Sodium Orthovanadate (Sigma), 10mM Na-β-glycerophosphate (Sigma), 5mM pyrophosphate (Sigma), protease inhibitors (Roche).

Western Blot

- **Acrylamide Bis-acrylamide solution** (29:1) (Amresco).
- **Resolving gel buffer** (pH=8.8)**:** 1.5M Tris-HCl (Sigma), 0.4% SDS (USB).
- **Stacking gel buffer** (pH = 6.8): 0.5M Tris-HCl, 0.4% SDS.
- **Loading buffer (5x):** 20% glycerol (Panreac), 10% SDS, 0.32% 2-β-mercaptoethanol (Sigma), 0.02% bromophenol blue (Sigma).
- **Electrophoresis buffer 1x:** 25mM Tris-HCl, 192mM Glycine (Serva), 1% SDS.
- **Transfer buffer:** 25mM Tris, 190mM glycine, 20% methanol.

3.7. Bacteria Transformation by Heat Shock

DNA constructs were amplified through transformation of chemically competent bacteria (*E.coli* TOP10^{R}, Invitrogen) by heat shock. All the procedure was carried near the Bunsen flame to avoid contaminations. Bacterial competent cells stored in 100µL aliquots at -80ºC were thawed in ice for 10 minutes. 0.50µL of DNA preparation was added to the cells and maintained in ice for 30 minutes. The thermal shock was carried out by incubating the tube at 42ºC for 90 seconds. 900µL of liquid LB medium (*Miller's LB Broth*, Conda) was then added and the mix was homogenized in the shaker at 37ºC for 1 hour. This allows cells to start expressing the plasmid encoded genes, including the antibiotic resistance. In order to concentrate the grown bacteria, the culture was centrifuged at 3000rpm for 5 minutes, and 800µL of supernatant was discarded. Cells were resuspended in the remaining supernatant and seeded in LB-agar (*Miller's LB Broth*, Conda), agar (Panreac) plate (Nunc) with the pertinent antibiotic, previously warmed at 37ºC. Cells were incubated at 37ºC overnight. Only transformed cells - containing the plasmid and thus the resistance to the antibiotic - were supposed to grow. Once transformed bacteria were grown,

colonies were picked and individually cultured in 3mL of liquid LB medium with antibiotic. These pre-cultures were incubated at 37ºC overnight in the shaker.

3.8. Minipreparations of plasmidic DNA

DNA minipreparations were performed to obtain plasmidic DNA by alkaline lysis of a bacterial pre-culture. This method provides low amounts of plasmidic DNA (5-15µg) with low purity. Nevertheless, it is enough for restriction-enzyme digestions carried out for plasmid verification.

1.5mL of bacteria culture was centrifuged at 12,000g for 1 minute. Supernatant was discarded and cells were suspended in 200µL of P1 (resuspension buffer). 400µL of P2 was then added and incubated at room temperature for 5 minutes, in order to lyse cells. 400µL of P3 was added in ice for neutralizing the mix and for protein precipitation. After centrifuging at 12000g for 10 minutes, supernatant was recovered and protein precipitate was discarded. DNA precipitation was achieved by adding 0.6 volumes (550µL) of isopropanol (Panreac), mixing, incubating at room temperature for 5 minutes and finally centrifuging at 9000g for 10 minutes. Supernatant was discarded and DNA pellet was washed with 500µL ethanol (Panreac) 70% v/v. After centrifugation at 12,000g for 5 minutes, supernatant was discarded and the pellet was dried until the remaining ethanol was evaporated. Finally, the DNA pellet is resuspended in 30µL of milliQ water with RNAseA (QIAGEN).

3.9. Maxipreparations of plasmidic DNA

DNA maxipreparations were performed to obtain large amounts of high-quality plasmidic DNA (250-1000mg). 200µL of transformed cultured bacteria were inoculated in a higher volume (250mL) of liquid LB medium with the pertinent antibiotic and grown in the shaker at 37ºC overnight. The DNA extraction was then carried out using the kit *E.Z.N.A™ Fastifilter* (Omega Bio-Tek), following the manufacturer's instructions. In short, this method is based in the alcaline lysis of cells with potassium acetate solution. DNA is purified by ionic exchange chromatography and precipitated with isopropanol. The purified DNA is resuspended in 500µL of milliQ water and concentration was determined by spectrophotometry (section 8.1).

3.10. Restriction enzyme digestions

Enzymatic digestions of DNA were performed using restriction endonucleases manufactured by Fermentas and/or New England Biolabs. Between 1 and 10 units (U) of restriction enzyme were used to digest 1 to 2 µg of plasmidic DNA, adding the buffer recommended by the manufacturer. Autoclaved milliQ water was added to reach the final volume fixed. For digestion reaction, Epperdorf tubes containing this mix were incubated at 37ºC, overnight.

3.11. DNA electrophoresis in agarose gel

3.11.1. Agarose gel preparation

Agarose 1% (w/v) gels were prepared in an Erlenmeyer flask by dissolving 1.80g of agarose (*Seaken LE Agarose*, Iberlabo) in 180mL of TAE 1x, heating the mix in a microwave. RedSafe™ Nucleic Acid Staining Solution 20.000x (iNtRON Biotechnology) was added to the flask when the agarose solution was tempered. RedSafe™ emits green fluorescence when it binds to DNA, becoming a non-carcinogenic alternative to ethidium bromide staining, typically used for DNA

display. The solution was then poured into the gel tray (BioRad), and once the gel polymerized, the comb was removed.

3.11.2. DNA electrophoresis

The agarose gel was placed into the electrophoresis cuvette and covered by TAE 1x solution. Loading buffer 10x was added to the DNA samples, and each one was loaded inside a gel well, leaving one well for the DNA Ladder (*GeneRuler 1kb*, ThermoFisher Scientific). An electric current of 70-100 V was applied for 45-60 minutes (*Sources of Power Pac Basic electrophoresis*, BioRad). The gel was then placed in a UV transiluminator (*GeneGenius BioImaging System*, Syngene) to display separated DNA fragments, and images were captured with the *GeneSnap* software (Syngene).

3.12. DNA purification from agarose gel

DNA fragments separated by electrophoresis were purified from agarose gels using the *GENECLEAN® Turbo Kit* (Q-BIOgene) following the protocol supplied by the manufacturer. This method is based on the ability of DNA to bind to a silica matrix. Purified DNA is finally suspended 30µL of nuclease free water (provided by the kit).

3.13. DNA defosforilation

In order to avoid that linealized pGV vector was recircularized because of 5' - 3' ends relegation, they were defosforilated using a Thermosensitive Alkaline Phosphatase. 1U of FastAP™ (Fermentas) and the buffer recommended by the manufacturer (Buffer FastAP 10x, Fermentas) were added to the purified pGV linealized vector and incubated at 37ºC for 10 minutes. After that, enzymes were inactivated at 75°C for 5 minutes.

3.14. DNA quantification

3.14.1. NanoDrop

Plasmidic DNA obtained from mini and maxipreparations was quantified by UV absorption at a wavelength of 260nm ($OD_{260/280}$). 2µl of the DNA preparation were loaded in the spectrophotometer NanoDrop ND-1000 (Thermo Scientific), which provides DNA purity and concentration in ng/µL.

3.14.2. Agarose gel Electrophoresis

Digested gel-purified DNA solutions were approximately quantified by electrophoresis in 1% agarose gel. 1µL of loading buffer was added to a volume of 6µL of DNA preparation, and then loaded into a gel well. 6µL of DNA Ladder GeneRuler 1kb (ThermoFisher Scientific) was loaded into an adjacent well. After electrophoresis, each DNA band was compared to the nearest band of the ladder, as they molecular length would be similar, thus the amount of retained dye would be comparable (the longer is a dsDNA molecule, the more dye is retained). The relationship of intensity between both bands is visually estimated, and the DNA concentration is calculated taking into account the ladder band concentration provided in the manufacturer's reference.

3.15. Ligation reaction

Ligation reaction to clone the insert (hKLS) into the expression plasmid (pGV) was catalyzed by the T4DNA ligase (New England Biolabs). This enzyme allows to bind DNA fragments with cohesive or blunt ends, by catalyzing the formation of two covalent phosphodiester bonds between 3' hydroxyl ends of one nucleotide with the 5' phosphate end of another, in an ATP-dependent manner. Ligation solutions were prepared in a total volume of 15µL, using 10U of ligase, ligase buffer 10x and 20ng of pGV vector. The final volume was reached by adding milliQ water. Ligation reactions took place at 16ºC, overnight. Enzymes were then inactivated at 65°C for 20 minutes.

3.16. Transient Transfection of HEK-293 cells with PEI

There are several procedures by which DNA can be introduced into a host cell. The chosen method was transient transfection with polyethylenimine (PEI), a stable cationic polymer that condenses DNA into positively charged particles that bind to anionic cell surfaces. Consequently, the DNA:PEI complex is endocytosed by the cells and the DNA is released into the cytoplasm (Sonawane, Szoka, & Verkman, 2003). This way, it is achieved the transient genetic expression based on episomal plasmid DNA expression, whose product is harvested after 48-72 hours post transfection.

Transfection of the expression vector was carried out in HEK-293 QB cells (ATCC® CRL-573TM, Q-BIOgene) in 6-well plates. To achieve an efficient transfection, cells must be in 50-70% confluence, so they were cultured the day before transfection in **growth medium** (DMEM) (Labclinics), supplemented with 10% (v/v) of FBS (Labclinics) and 1% (v/v) of antibiotics Penicillin/Streptomycin (Labclinics).

For one well (1,2x10^6 cells), 6µg of plasmidic DNA were transfected. To this end, two different solutions were previously prepared in excess.

- On one hand, 15µg of plasmidic DNA were dissolved in 300µL of NaCl 0.9% (B.Braun).
- In a different tube, PEI 10mM (PolyScience) was mixed in NaCl 0.9% (using 2.25µL of PEI per µg of DNA) in a final volume equal to that of the DNA solution (300µL).

In order to get the DNA:PEI complexes formed, the PEI solution was carefully added, drop by drop, into the DNA tube and incubated at room temperature for 20 minutes. Culture medium was then aspirated and transfection medium (DMEM + 1% FBS, without antibiotics) was added to the cultured cells (500µL per well). After that, the DNA:PEI mix was added (240µL per well) and plates were incubated at 37ºC and 5% CO_2 for 3 hours. To avoid PEI-related toxicity, the medium was removed and growth medium was added. Plates were incubated at 37ºC and 5% CO_2 for 72 hours to let the plasmid be expressed inside cells, thus producing the coded protein.

In order to ensure sterility, all the experiments using cell cultures were carried out in level 2 biosafety laboratories, using a laminar flow cabinet with UV light system (Telstar).

3.17. Protein extraction

Proteins produced by HEK-293QB transfected cells were extracted by cell lysis using RIPA buffer and a sonicator VCX130PB 130 watts (*Sonics*, Newtown, USA). Samples were kept in ice during every stage of the process in order to preserve protein integrity. 500µL of RIPA buffer was added to each cell sample (composed of cell extracts from 2 wells of similar conditions). Then cell samples were sonicated in three cycles. Each cycle consisted on 3 pulses of 3 seconds of

sonication at 40 kHz. Lysed cells were centrifuged for 15 minutes at 13200 rpm and 4ºC. Supernatant was transferred into a new Eppendor tube and stored at -20ºC until protein quantification.

3.18. Protein quantification

Protein extracts were quantified through the Bradford's method (Bradford, 1976) using the *Pierce BCA Protein Assay Kit* (Thermo Scientific), which is a colorimetric assay based on the biuret reaction (reduction of Cu^{+2} to Cu^{+1} by protein) and the detection of Cu^{+1} using a bicinchoninic acid (BCA). This complex formed exhibits a strong absorbance at 562nm that is nearly linear with increasing protein concentrations over a broad working range (20-2000µg/mL). Protein concentrations are determined using a reference to standards of a common protein, bovine serum albumin (BSA) and spectrophotometry. In order to establish the standard curve, serial dilutions of BSA stock solution 2mg/mL (supplied by the kit) were prepared using milliQ water, consisting on final BCA concentrations of 0 – 1500 – 1000 – 750 – 500 – 250 - 125 - 25 - 0 (blank) µg/mL.

Protein samples were diluted in milliQ water at 1:5, which is a suitable dilution for quantification of protein produced by cultured cells. Protein samples and standard solutions were loaded into a 96-well microplate, per duplicate (10µL per well). 200µL of *working solution* (supplied by the kit) was added to each well. The microplate was then incubated for 30 minutes at 37ºC. Absorbance at 562nm was determined by *the Absorbance Reader ELx808* (BioTek) and analyzed using the *KC4 software* (BioTek).

3.19. Protein analysis by Western Blot

3.19.1. Protein sample preparation

A volume of protein solution containing 15µug of protein extract (based on the measured concentration) was mixed with 5uL of loading buffer 6x, and milliQ water was added to reach a final volume of 30µL. Proteins were denatured at 99ºC for 10 minutes (*Eppendorf Thermomixer R 5355 w/ MTP Microplate Thermoblock Heater Mixer Shaker*, BioRad), and stored at -20ºC.

3.19.2. Protein Electrophoresis in denaturing Polyacrylamide Gel

The proteins contained in each sample were separated according to their molecular weight through sodium dodecyl sulphate polyacrylamide gel electrophoresis (SDS-PAGE). SDS is an anionic detergent that denatures proteins, which lose their three-dimensional structure. Then, when applying and electric field, proteins migrate according to their molecular weight.

Gels for protein separation were prepared at 10% acrylamide in resolving gel buffer. A stacking gel at 5% acrylamide was prepared using stacking gel buffer. This is the part of the gel in which wells are formed, and allows protein concentration in the well prior to separation. For gel polymerization, APS 10% (Amresco) and terametil-etilen-diamina (TEMED) (Sigma), at 5:1 proportion, were added to both solutions.

Polymerized gel was placed into the electrophoresis chamber *Mini Protean Tetra Cell* (BioRad), and totally covered with electrophoresis buffer 1x. 30µL of protein sample was loaded in each gel well using a Hamilton syringe (*Hamilton Microliter™ Syringes*, Hamilton). In order to identify each protein band according to its size, the molecular weight marker *Page-Ruler Prestained Protein Ladder* (Fermentas) was loaded into a different well.

Protein samples were run in two cycles: first at 90V for 20 minutes (to concentrate proteins in the wells before entering into the separating gel fraction) and then at 130V for 1h30min (for protein separation), using the *PowerPac Basic Power Supply* (BioRad).

3.19.3. Transference

Once proteins were separated in the gel, they were transferred onto a PVDF blotting membrane (GE Healthcare Life Sciences). This membrane was previously activated with methanol *HPLC grade* (Sigma) during 10 seconds, washed with distilled water and then maintained in transfer buffer. Two Whatman papers (*Extra Thick Western Blotting Filter Paper*, Thermo Scientific) and the gel containing the separated proteins were wetted in transfer buffer for 15 minutes before transference. All components were placed on the transference device (*Bio-Rad Trans-Blot SD Semi-Dry Transfer Cell*, BioRad), in this order: one Whatman paper, the activated PVDF membrane, the gel containing the separated proteins and finally the second Whatman paper. A pin was rolled after placing every layer to eliminate bubbles that could alter the electric current, thus affecting the correct protein transference to the membrane. The transference was carried out by applying an electric current of 30V for 45 minutes.

3.19.4. Immunodetection

3.19.4.1. Blocking

In order to avoid unspecific bindings of the primary antibody, the transferred membrane was blocked in blocking solution (5% w/w BSA in TBST buffer), during 1h30min at room temperature in a shaker.

3.19.4.2. Primary antibody incubation

The primary antibody (K-18.2) used in this experiments to recognise the hKLS protein had been designed by our group and produced by EZBiolab (Carmel, USA) on rabbits. Lyophilized antibody was reconstituted in a final volume of 25mL using ultrapure water (Braun) and stored in aliquots of 100µL and 1mL at -20ºC.

Antibody dilutions were prepared with 5% BSA blocking solution, and used for membrane incubation at 4ºC overnight in gently agitation.

After incubation, the antibody solution was recovered and the membrane was washed in TBST solution undergoing three fast washes followed by one 10-minute wash and three rounds of 5-minute washes in a shaker.

3.19.4.3. Secondary antibody incubation

Washed membranes were incubated for 1 hour at room temperature with the secondary antibody (*Polyclonal Swine Anti-Rabbit Ig/HRP*, Dako Cytomation), diluted 1:10000 in 5% BSA. This is an anti-rabbit antibody conjugated to the peroxidase enzyme (HRP) that allows specific protein detection. After incubation, the membrane was washed using TBST solution, undergoing 2 fast washes and 3 rounds of 12-minute washes in a shaker.

3.19.4.4. Signal detection

In order to detect the specific recognition of the protein of interest by the primary antibody, the membrane was incubated for 5 minutes with horseradish peroxidase-luminol reagents of *Immobilon™ Western Chemi-luminiscent HRP Substrate* (*Millipore*): *HRP Substrate Peroxide*

Solution and *HRP Substrate Luminol Reagent*, previously mixed 1:1. The peroxidase enzyme conjugated to the secondary antibody catalyzed luminol oxidation by the peroxide, and oxidized luminol emitted light that was detected through a chemiluminiscence system (*ChemiDoc*, BioRad). Images were obtained and analyzed with *QuantityOne 1-D* analysis software from BioRad.

4. RESULTS AND DISCUSSION

4.1. pEX+hKLS plasmid amplification and verification

The synthetic plasmid containing the hKLS gene (pEX+hKLS) was amplified by DNA maxipreparation after transformation of *E.coli* competent bacteria. Restriction digestions were performed using three specific endonucleases (PvuII, PstI) in order to ensure that the amplified DNA corresponded to the pEX+hKLS plasmid, whose digestion products were predicted using the program *DNA Strider v1.4f4 for Macintosh* (**Table 1**).

For each digestion reaction, between 3 and 6 U of restriction enzyme were used to digest 1µg of DNA obtained from the maxipreparation, in a final volume of 20µL, under the conditions detailed in section 3.10. After restriction digestions, DNA fragments were separated by electrophoresis in agarose gel.

As it can be observed in **Figure 5**, digestions using PvuII enzyme resulted in one DNA fragment above the 2500bp band of the marker and another at the level of 1000bp, in agreement with the 2579bp and 1001bp expected fragments. Smaller expected bands (360 and 235bp) are not detected in this gel, as happens for the marker (bands smaller than 700bp are not visible). Despite PstI digestion was not completely effective, the expected bands of 2549bp and 1377bp can be identified in this picture.

These results confirmed that the amplified plasmid was the pEX-hKLS, allowing us to go on with the cloning process.

***Table 1*. Expected size of DNA fragments after digestion of pEX+hKLS plasmid with restriction enzymes (PvuII and PstI).** DNA size measured in bp (base pairs).

Enzyme	PvuII	PstI
Expected DNA fragments (bp)	2579 1001 360 235	2549 1377 249

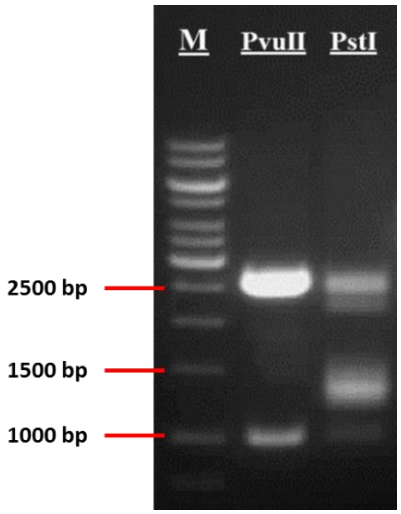

***Figure 5*. Electrophoresis of DNA fragments resulting from digestion of amplified pEX+hKLS plasmid with PvuII and PstI enzymes**. M: marker (DNA Ladder).

4.2. *hKLS* cDNA isolation and pGV plasmid linearization

Enzymatic digestions were then performed:

a) to isolate the hKLS gene from the pEX+hKLS synthetic plasmid, and
b) to linearize the pGV plasmid.

The restriction enzymes used (**Table 2**) generate complementary ends, thus facilitating the binding between the hKLS fragment and the pGV linearized plasmid in the ligation reaction.

Table 2. **Restriction enzymes used to cleave each plasmid and expected DNA fragments generated.**

Plasmid	Restriction enzymes	Expected DNA fragments (bp)
pEX+KLS	XbaI + NotI	2492 1656 (hKLS insert) 15
pGV	NheI + NotI	4914 (linealized plasmid) 79

After digestions, DNA fragments were separated by agarose gel electrophoresis (**Figure 6**). As shown in **Figure 6.a**, the hKLS insert (1656bp) could be identified above the level of 1500bp while the remainder pEX plasmid (2492bp) was around the level of 2500bp. The 15bp band expected from pEX+hKLS digestions was not visible due to its small length. Likewise, the pGV linearized plasmid (4914bp) was visible at the level of 5000bp (**Figure 6.b**), but the 79bp-band could not be identified.

Bands belonging to the hKLS insert and the linearized pGV (marked in blue in figure) were isolated and purified from the gel following the protocol detailed in section 3.12).

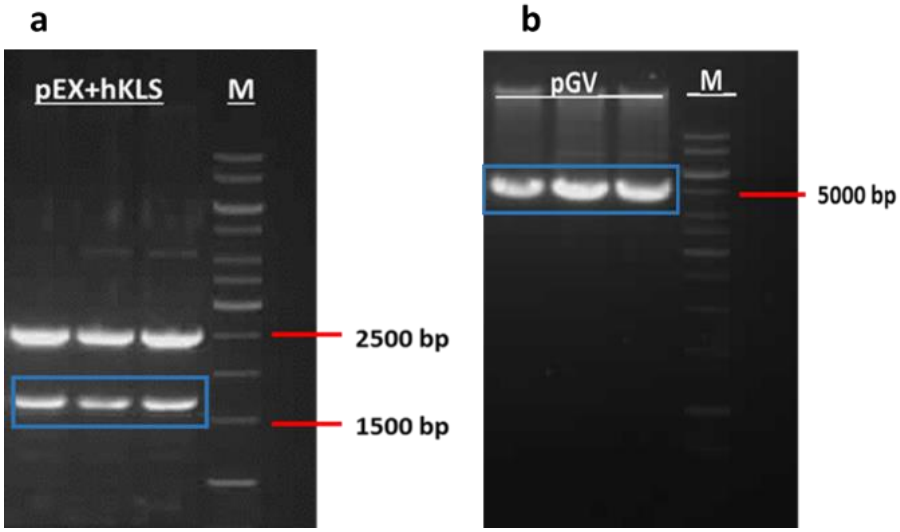

Figure 6. **DNA fragments resulting from enzymatic digestions of pEH+KLS** (a) **and pGV** (b) **plasmids.** The bands marked in blue correspond to the hKLS isolated cDNA (a) and the linealized pGV plasmid. M: marker (DNA Ladder).

Linearized plasmids are prone to undergo re-circularization during ligation reaction when they have been previously digested with a single restriction enzyme, or with two enzymes with compatible ends. This was not supposed to be likely to happen in the pGV plasmid, given that its linearization had been done using two restriction enzymes (NheI and NotI) which do not generate complementary ends. However, partially-digested linear pGV plasmids could be present in the solution and spontaneously re-ligate during the ligation reaction. The resulting pGV re-circularized plasmid would highly decrease the efficiency of the hKLS-pGV ligation, and it would also give false positive colonies after bacteria transformation. To avoid this, the linearized pGV vector was dephosphorylated following purification from the agarose gel.

4.3. hKLS and pGV DNA quantification

In order to fix the different conditions of the ligation reactions, hKLS and pGV concentrations had to be known. To this end, 6µL of each DNA solution were used to determine their concentration by electrophoresis in agarose gel (**Figure 7**), following the method detailed in section 3.14.2).

The hKLS band showed approximately the double intensity than it nearest band of the ladder (1500bp; 10.00 ng/µL). Thus, the hKLS concentration in the solution was estimated to be about 20 ng/µL. In the same way, the pGV band seemed to be four times more intense than the 6000bp ladder band (11.67 ng/µL), so the pGV concentration in its solution resulted in 46.67 ng/µL.

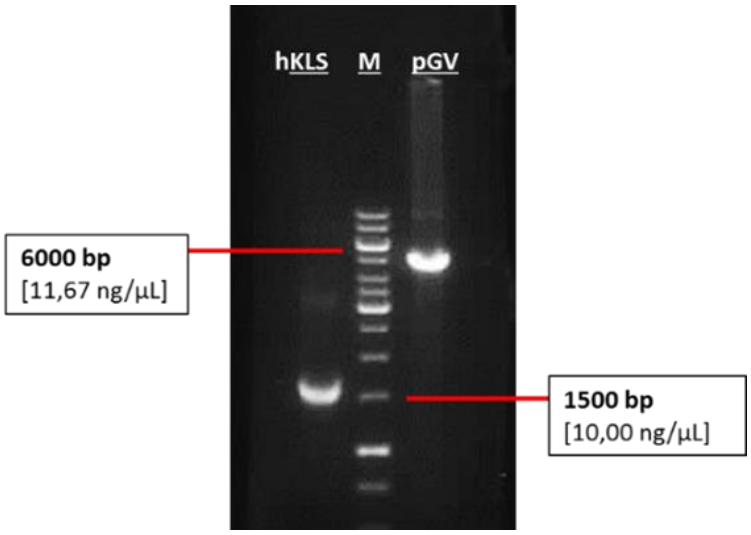

Figure 7. **Electrophoresis of hKLS and pGV DNA for quantification.**

4.4.Verification of pGV+hKLS ligation

For the ligation reaction, different standard vector:insert proportions were tested: one containing equimolar amounts of both DNA fragments (1:1) and another with higher amount of insert (1:3). One reaction without insert (1:0) was used as a control of the phosphatase efficiency.

Ligations were verified by transforming chemically competent bacteria. As expected, when seeded into LB-agar plates, only bacteria transformed with ligations 1:1 and 1:3 grew.

Several colonies were picked from 1:1 and 1:3 plates and grown in liquid LB medium. Plasmidic DNA was extracted by minipreparation from every cultured colony and the correct orientation of

the insert into the vector was validated using specific restriction enzymes (**Table 3**) and electrophoresis in agarose gel (**Figures 8** and **9**).

Plasmidic DNA extracted from colony 7 showed a positive result for both restriction reactions:

Digestion using PvuII (**Figure 8**) produced a band at the level of 3500bp and another below 2500 bp, which probably corresponded with the expected bands: 3639 and 2437 bp.

Likewise, digestion with EcoICRI (**Figure 9**) resulted in a band between 6000 and 5000bp, feasibly corresponding to the expected band of 5831bp.

Expected smaller bands were not visible in this gel. However, the presence of the previously cited bands, together with the absence of other exclusive bands expected from different constructs (for instance, 1362bp, 4892bp and/or 2579bp), provide enough evidence to confirm that the colony 7 was transformed with the pGV+hKLS vector.

***Table 3*. Expected DNA fragments (bp) obtained after restriction enzyme digestion (with PuvII and EcoICRI), depending on the DNA construct amplified:** pGV+hKLS vector (positive result), pGV or pEX+hKLS (negative results).

Enzyme	pGV+hKLS	pGV	pEX+hKLS
PvuII	3639 2437 502	3639 1362	2579 1001 360 235
EcoICRI	5831 507 240	4892 109	3935 240

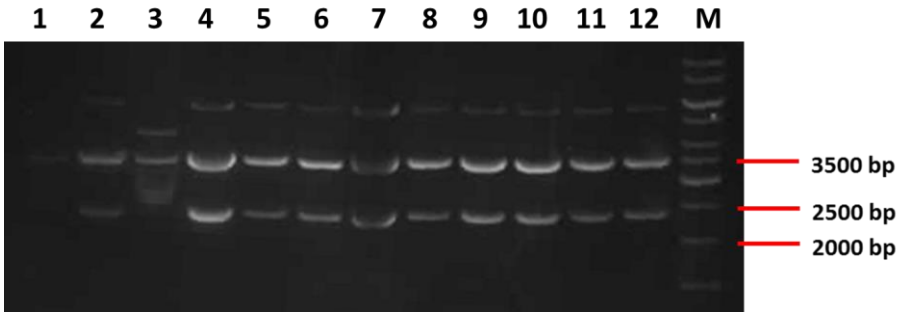

***Figure 8.* DNA fragments resulting from digestion with PvuII enzyme. M: marker (DNA Ladder).**

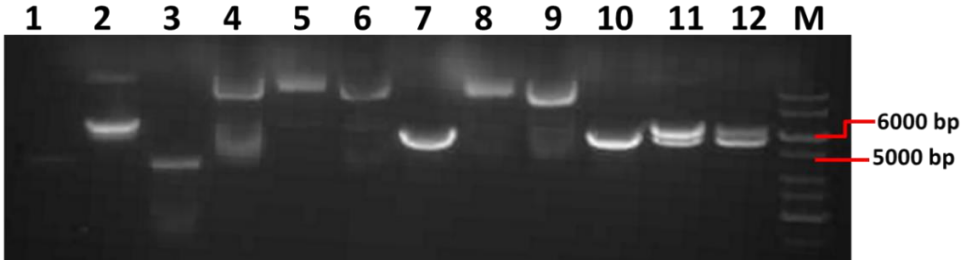

***Figure 9.* DNA fragments resulting from digestion with EcoICRI enzyme. M: marker (DNA Ladder).**

Then, with the aim of amplifying the pGV+hKLS plasmid, colony 7 was cultured in a higher volume of liquid LB medium. The plasmidic DNA was then extracted by maxipreparation and quantified using *Nanodrop*, resulting in 682.9 ng/µL. The obtained pGV+hKLS vector was sufficient for subsequent transfection in cultured mammalian cells, and for storage for future applications.

Given the variety and importance of the future applications for the amplified vector, it was worth verifying the pGV+hKLS identity once again through a battery of different restriction enzyme digestions (**Table 4**) followed by electrophoresis in agarose gel. As it can be observed in **Figure 10,** all expected bands beyond 352bp were clearly visible for the different restriction enzyme digestions, despite the bands of 352, 502 and 507bp expected from digestions with SnaBI, PvuII and EcoICRI, respectively. These are not easily identified in this picture due to its low quality, although they were detected in screen when the gel was analyzed in the UV transiluminator.

Together, these results confirmed that the amplified plasmid corresponded to the pGV+hKLS, which could be used from this point onwards for different applications.

Table 4. **Expected DNA fragments (in bp) when digesting pGV+hKLS or pGV with different restriction enzymes.**

Enzymes	XmaI	SnaBI	XmaI + SnaBI	PvuII	EcoICRI
pGV+hKLS	3698 1761 1085 7	3974 2252 352	3698 1638 610 352 123 7	3639 2437 502	5831 507 240
pGV	3698 1273 7	3974 675 352	3698 675 352 123 7	3679 1362	4892 109

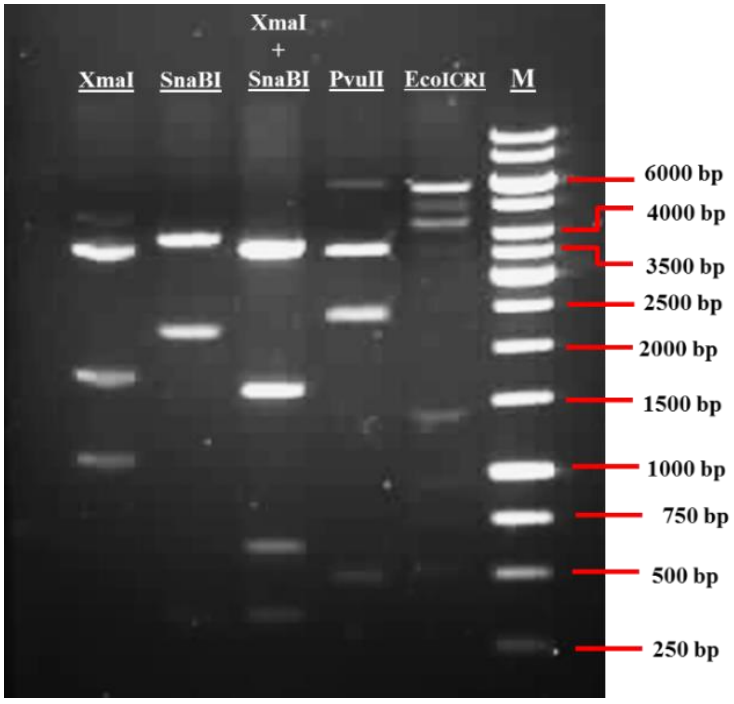

Figure 10. **Electrophoresis of DNA fragments resulting from verification digestions of the amplified vector.**

4.5. Transient transfection of HEK-293 cell line with the pGV+hKLS vector.

Transfection is the process of introducing exogenous nucleic acids by non-viral methods into eukaryotic cells. With the aim of producing the hKLS protein in vitro, HEK-293QB cells were transfected with the expression vector pGV+hKLS through the PEI method.

Apart from transfecting HEK-293QB cells with the pGV+hKLS vector (a), other different conditions were established as controls:

(b) HEK-293QB cells transfected with the pGV plasmid, without genes cloned (pGV).

(c) HEK-293QB cells transfected with the pDsRed2-Mito Vector, encoding the red fluorescent protein DsRed2 (pDsRed2-Mito).

(d) HEK-293QB cells non-subjected to transfection procedure (NT).

72 hours following transfection (time enough for the plasmids to be expressed), cells were observed in a Nikon fluorescence microscope connected to a camera (*Digital Sight DS-U1*, Nikon). Photographies of cells in plates (**Figure 11**) were taken in both clear field (**1**, upper row) and also using a red fluorescence filter (**2**, lower row).

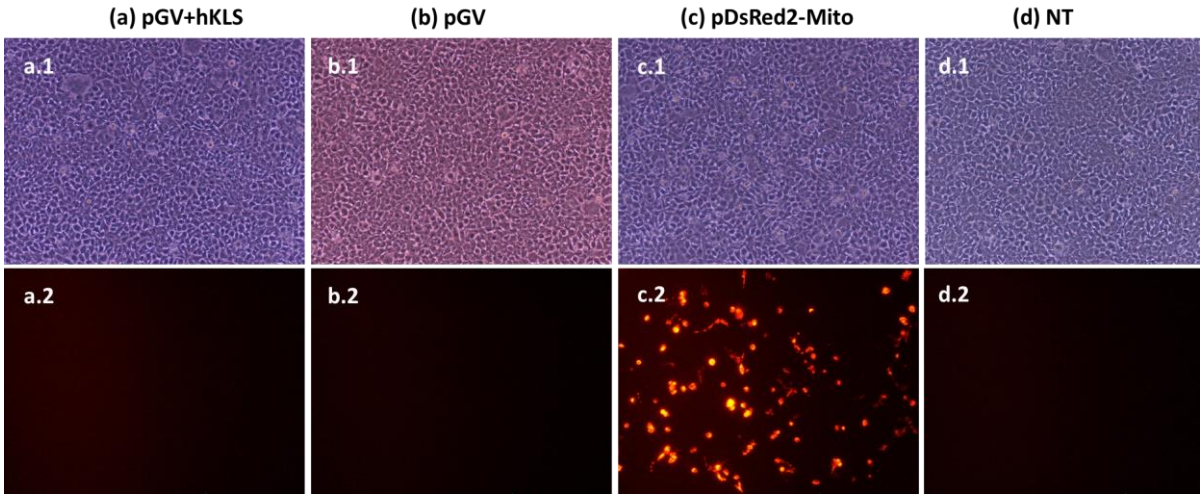

Figure 11. **Photographies of cultured cells in clear field** (1) **and under a fluorescence filter** (2)**.**
(a), (b) and (c) were transfected with pGV+hKLS, pGV and pDsRed2-Mito plasmids, respectively. (d): Non-transfected cells (control).

Cells non-subjected to the transfection procedure (**d.1**) were used to confirm that the culture conditions were suitable. In case of growth anomalies in the other conditions, these would be inherent to the transfection process.

Cells transfected using the pDsRed2-Mito plasmid showed red fluorescence when the filter was applied (**c.2**), indicating that the transfection was effective and the introduced plasmid was being expressed.

As expected, any other plate showed red fluorescence when the red filter was applied (**a.1**, **b.2**, and **d.2**), as none of them contained any gene coding for a fluorescent protein.

The hKLS protein, coded in the pGV vector, did not appeared to be toxic for cells, as no differences in growth are observed in plate **a.1** compared to the other conditions.

Likewise, any toxicity related to the DsRed2 fluorescent protein was observed (**c.1**).

4.6. Quantification of protein extracts from HEK-293 cells

Once protein extracts were obtained from cultured cells, its concentration was determined using the BCA colorimetric assay and spectrophotometry, following the method explained in section 3.18.

From the BSA dilutions of known concentration, a standard curve (**Figure 12**) was obtained with a R^2=0.978, which implies the model is highly reliable.

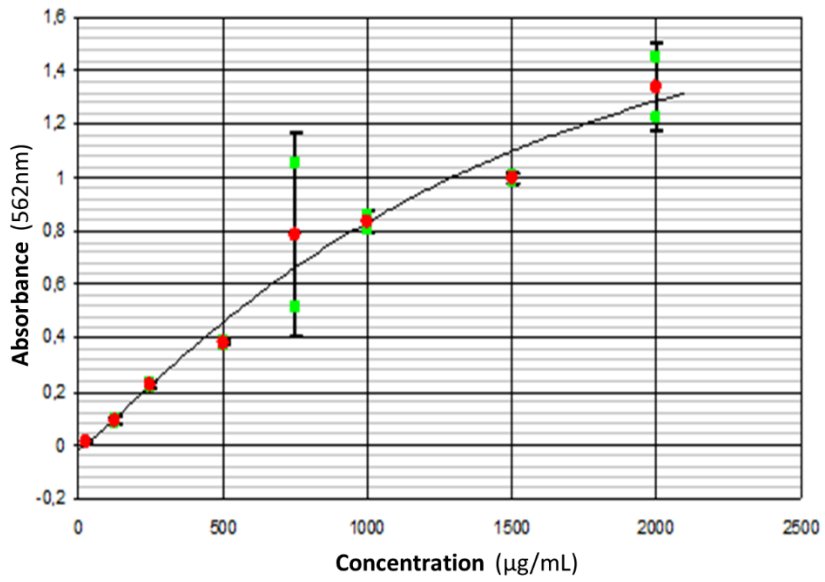

Figure 12. **Standard curve of BSA for protein quantification.** BSA standards of known concentration, ranging from 0 to 1500 µg/mL, are loaded (x-axis) and their absorbance at 562nm is measured (y-axis).

The graph represents the absorbance value as the dependent variable (Y-axis) and concentration as the independent variable (X-axis), through the equation:

$$y = \frac{a-d}{1+(\frac{x}{c})^b} + d \qquad \textit{(Equation 1)}$$

whose obtained parameters are shown in **Table 5**:

Table 5. **Standard curve fitting results.**

a	b	c	d	R	R^2	Err.
-0.014	1.184	1510.91	2.22	0.989	0.978	0.065

Fitting the obtained parameters in Equation 1, Equation 2 is obtained and used to determine protein concentration (x) of an unknown sample by inserting the sample's absorbance value (y) and solving for x.

$$y = \frac{-2.234}{1+(\frac{x}{1510.91})^{1.184}} + 2.22 \qquad \textit{(Equation 2)}$$

Concentration of protein samples was calculated taking into account their dilution. The resulting value was obtained as the mean of the both replicas loaded for each sample (*Mean* column).

Table 6. **Protein concentration calculated for each cellular extract.**

Well ID	Conc.\Dil.	Concentrations	Concentrations x Dil.	Mean (µg/mL)	Std Dev	CV (%)
pGV+hKLS (a)	5	174.728 175.715	873.64 878.576	**876.108**	3.491	0.398
pGV (b)	5	170.778 163.861	853.89 819.307	**836.599**	24.454	2.923
pDsRed2-Mito (c)	5	165.838 151.986	829.191 759.928	**794.56**	48.976	6.164
Non transfected (d)	5	159.906 160.895	799.53 804.475	**802.002**	3.497	0.436

Quantification of protein extracts reveals that there are not great differences in the protein production between the different conditions established. The transfected DNA construct and the protein produced do not seem to be toxic for cells, since its concentration is similar to that of the controls, as expected.

4.7. hKLS protein analysis by Western blot

4.7.1. Optimization of K-18.2 antibody protocol using protein extracts from mice

One of the main goals of this work was to get to analyze the hKLS protein obtained from human samples using the K-18.2 antibody, specially designed for it. As human samples are limited and highly valuable, and the K-18.2 antibody had never been used before, its optimal conditions were established using the mKLS protein, present in murine protein samples available in our laboratory.

4.7.1.1. Determining optimal antibody variant and dilution

K-18.2 antibody was produced in two different rabbits (whose antibody extracts were named #1# and #2#, respectively). In order to determine which antibody variant was more specific for the KLS protein, they both were tested with brain protein extracts from three different mice.

Ab K-18.2 from rabbit #1# recognized a protein at the level of about 20kDa, and the best dilution tested seemed to be the 1/5.000, as bands appeared more intense (**Figure 13**).

In contrast, Ab K-18.2 from rabbit #2# revealed multiple bands of higher molecular weight (**Figure 14**). Of great relevance were the bands at the level of 55-50 kDa, as similar results were obtained in previous studies carried out by our group, using the antibody K-113, specific for the murine s-KL (mKLS) (R. Notario, personnal communication). As for the optimal dilution, it seemed to be the 1/10.000, given that at higher concentration, Ab K-18.2 from rabbit #2# revealed more background and unspecific bands.

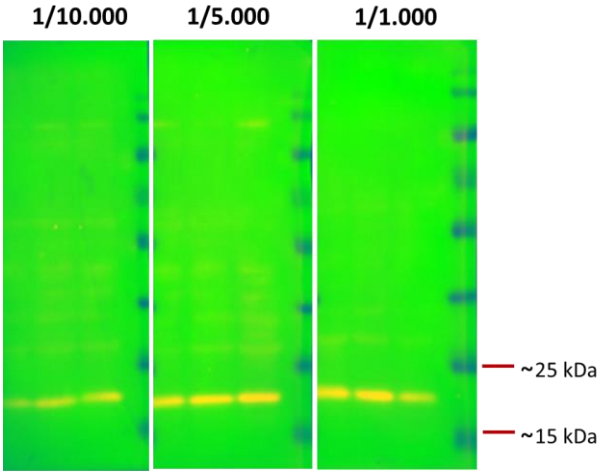

Figure 13. **mKLS immunodetection using variant #1# of K-18.2 antibody diluted 1/10.000, 1/5.000 and 1/1000.**

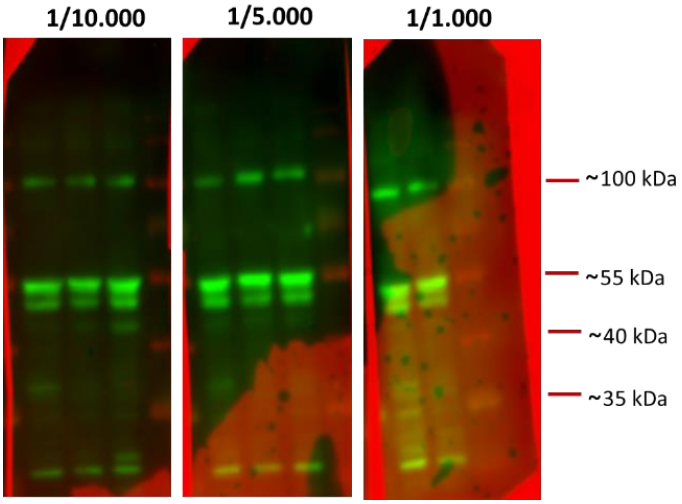

Figure 14. **mKLS immunodetection using variant #2# of K-18.2 antibody diluted 1/10.000, 1/5.000 and 1/1000.**

4.7.1.2. Evaluation of antibody specificity using an immunogenic peptide

In order to check whether the K-18.2 antibody was specific for the recognized proteins, it was pre-incubated with an immunogenic peptide (provided by the antibody manufacturer). This immunogenic peptide is highly specific for the K-18.2 antibody and competes with the other proteins in the membrane for it.

As **Figure 15** shows, no protein in the membrane was recognized by the K-18.2 antibody, neither #1# nor #2#, indicating that both variants did not recognize unspecific proteins in previous experiments. In other words, the K-18.2 does not detect random proteins, but it is specific for its target, KLS.

Therefore, since bands revealed by K-18.2 antibody from rabbit #2# seemed to be more prone to correspond to KLS, this variant was selected for the following experiments.

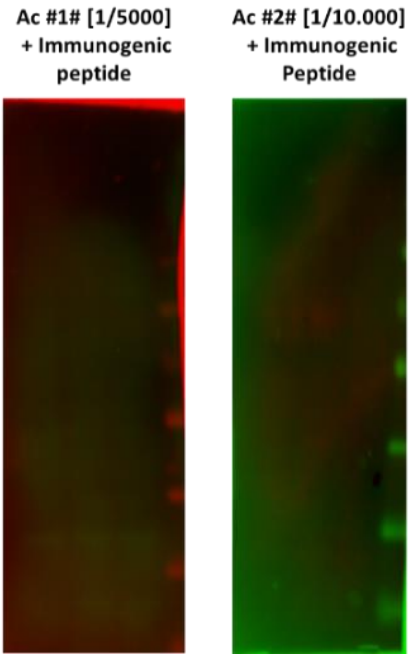

Figure 15. **Specificity test for K-18.2 antibody (#1: left; #2#: right): Immunodetection of mKLS after pre-incubation with specific immunogenic peptide.**

4.7.1.3. Background optimization for antibody K-18.2 #2#

Once the best variant and dilution of the K-18.2 antibody were established, we went one step further with the aim of eliminating the background and unspecific signals detected. To this end, different washing conditions were tested after incubating the membrane with the K-18.2 #2# antibody, diluted 1/10.000. In all cases, 3 fast washes followed by one ten-minute wash in agitation were firstly performed. After that, different washing conditions were tested (**Figure 16**).

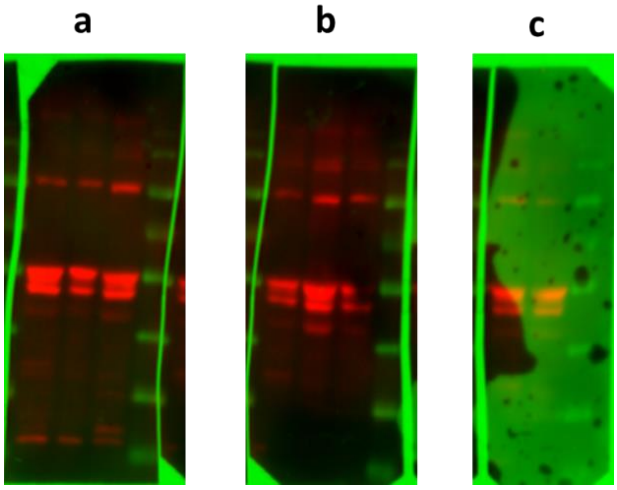

Figure 16. **Testing different washing conditions for antibody K-18.2 #2#.** (a): 1 five-minute wash, (b): 2 successive five-minute washes, (c): 3 successive five-minute washes.

Even if it might not be clearly visible in this picture, condition (c) resulted to be the most suitable for background and unspecific signals elimination, and therefore, this was the protocol established in the following experiments.

4.7.2. Analysis of human KLS protein (hKLS)

Once the optimal conditions for the K-18.2 antibody were established, Western Blot analysis were carried out using the human variant of the KLS protein (hKLS).

4.7.2.1. Analysis of the *in vitro* produced hKLS protein

On the one hand, we used the protein extracted from pGV+hKLS-transfected cells to verify the hKLS production. As control, we used the protein extracted from cells transfected solely with the pGV plasmid. As **Figure 17** shows, K-18.2 antibody recognised a prominent band at the level of 70kDa, which was not present in the pGV transfected cells. This, together with the fact that the molecular weight of the hKLS protein is 70kDa, indicates that this band corresponds to the hKLS protein. This experiment also revealed that the hKLS protein was highly produced by the transfected cells.

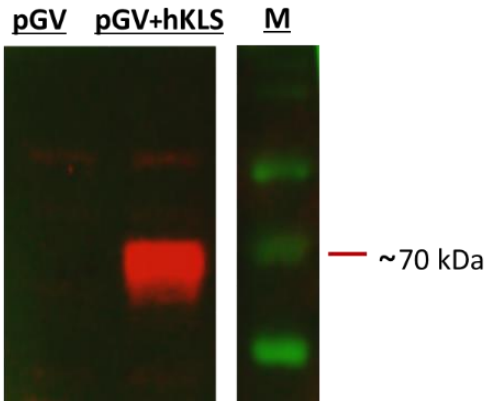

Figure 17. **Immunodetection of hKLS produced by transfected cells using the K-18.2 antibody.**

4.7.2.2. Analysis of hKLS from human brain samples.

On the other hand, protein extracts from human brains of both healthy and AD patients were analyzed using the K-18.2 antibody. These human brain samples were obtained from the biobanc of the Hospital de Bellvitge and processed in our laboratory to obtain the protein extracts.

The antibody detected three bands of around 55kDa, both in healthy and AD patients (**Figure 18**). However, these do not fit the expected 70kDa band of the hKLS protein. This is in agreement with previous results obtained by our group in mice experiments: when analyzing Klotho from brain samples with different commercial antibodies, several bands smaller than 70kDa appeared as well. Conversely, when analyzing protein extracts from kidney, only one band was obtained. Thus, we believe that hKLS suffers some kind of processing in the brain, but further research is needed to confirm it.

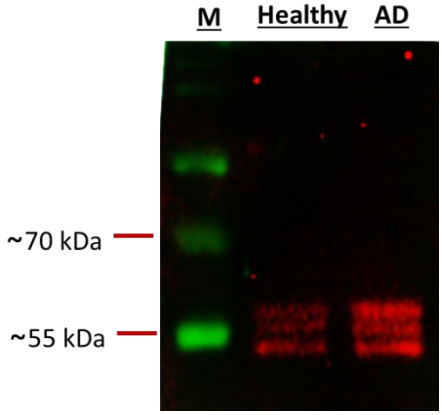

Figure 18. **Immunodetection of hKLS extracted from healthy and AD human brains using the K-18.2 antibody.**

4.7.2.3. Verification of K-18.2 specificity with human KLS

In order to confirm that the previous bands were not random recognitions of the K-18.2 antibody, the same protein extracts were analysed using the K-18.2 antibody pre-incubated with the immunogenic peptide.

The membrane containing the protein extracts from both human patients and transfected HEK-293 cells did not show any band (**Figure 19**) , indicating that the proteins recognized by the antibody K-18.2 in the previous experiments were specific, likely corresponding to some form of hKLS.

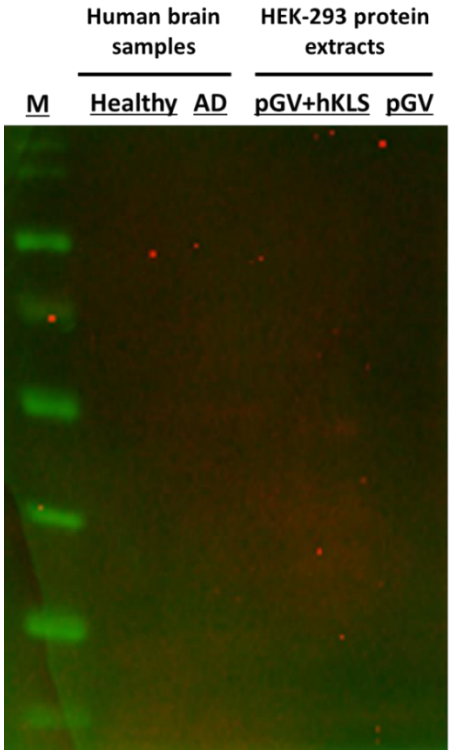

Figure 19. **Testing K-18.2 specificity for human KLS obtained from brain samples (Healthy and AD) and HEK-293 transfected cells (pGV+hKLS and pGV).**

5. CONCLUSION AND FUTURE APPROACHES

In this work the human s-KL (hKLS) gene has been successfully cloned in a eukaryote expression vector (pGV) by means of Molecular Biology techniques. When transfecting the obtained construct (pGV+hKLS) into HEK-293 cultured cells, it was highly expressed and the stable protein of 70kDa hKLS was produced, as expected. This protein allowed the validation of the new K-18.2 antibody, specifically generated by our group to detect the human s-KL protein. Thus, this work has provided us two important tools to continue our research:

- On the one hand, we have at our disposal the *in vitro* produced hKLS protein, which will be used to generate a calibration curve that allows the relative quantification of the protein extracted from human samples.
- On the other hand, we have optimized the protocol of the K-18.2 antibody to detect the human s-KL protein by Western Blot. In the future, an ELISA assay will be set up to quantify also s-KL in low concentration samples, for instance in CSF.

In this way, we will be able to correlate the levels of s-KL with the progression and severity of Alzheimer's disease, as well as with aging.

6. BIBLIOGRAPHY

Anand, R., Gill, K. D., & Mahdi, A. A. (2014). Therapeutics of Alzheimer's disease: Past, present and future. *Neuropharmacology*, *76*(PART A), 27–50.

Asai, O., Nakatani, K., Tanaka, T., Sakan, H., Imura, A., Yoshimoto, S., … Saito, Y. (2012). Decreased renal α-Klotho expression in early diabetic nephropathy in humans and mice and its possible role in urinary calcium excretion. *Kidney International*, *81*(6), 539–47.

Bektas, A., Schurman, S. H., Sharov, A. A., Carter, M. G., Dietz, H. C., & Francomano, C. A. (2004). Klotho gene variation and expression in 20 inbred mouse strains. *Mammalian Genome*, *15*(10), 759–767.

Bloch, L., Sineshchekova, O., Reichenbach, D., Reiss, K., Saftig, P., Kuro-o, M., & Kaether, C. (2009). Klotho is a substrate for alpha-, beta- and gamma-secretase. *FEBS Letters*, *583*(19), 3221–3224.

Bohnen, N. I., Kaufer, D. I., Hendrickson, R., Ivanco, L. S., Lopresti, B., Davis, J. G., … DeKosky, S. T. (2005). Cognitive correlates of alterations in acetylcholinesterase in Alzheimer's disease. *Neuroscience Letters*, *380*(1–2), 127–132.

Bradford, M. M. (1976). A rapid and sensitive method for the quantitation of microgram quantities of protein utilizing the principle of protein-dye binding. *Analytical Biochemistry*, *72*, 248–54.

BrightFocus Foundation (2016). *Protein aggregates in an Alzheimer's diseased brain.* Retrieved from http://www.brightfocus.org/alzheimers/infographic/amyloid-plaques-and-neurofibrillary-tangles.

Brookmeyer, R., Johnson, E., Ziegler-Graham, K., & Arrighi, H. M. (2007). Forecasting the global burden of Alzheimer's disease. *Alzheimer's and Dementia*, *3*(3), 186–191.

Butler, M., & Shelanski, M. L. (1986). Microheterogeneity of micro tubule-associated proteins is due to differences in phosphorylation. *Journal of Neurochemistry*, *47*(5), 1517–1522.

Chang, Q., Hoefs, S., van der Kemp, A. W., Topala, C. N., Bindels, R. J., & Hoenderop, J. G. (2005). The beta-glucuronidase klotho hydrolyzes and activates the TRPV5 channel. *Science*, *310*(5747), 490–493.

Chen, C.-D., Sloane, J. A., Li, H., Aytan, N., Giannaris, E. L., Zeldich, E., … Abraham, C. R. (2013). The Antiaging Protein Klotho Enhances Oligodendrocyte Maturation and Myelination of the CNS. *Journal of Neuroscience*, *33*(5), 1927–39.

Clinton, S. M., Glover, M. E., Maltare, A., Laszczyk, A. M., Mehi, S. J., Simmons, R. K., & King, G. D. (2013). Expression of klotho mRNA and protein in rat brain parenchyma from early postnatal development into adulthood. *Brain Research*, *1527*, 1–14.

Di Bona, D., Accardi, G., Virruso, C., Candore, G., & Caruso, C. (2014). Association of Klotho polymorphisms with healthy aging: a systematic review and meta-analysis. *Rejuvenation Research*, *17*(2), 212–6.

Dubal, D. B., Yokoyama, J. S., Zhu, L., Broestl, L., Worden, K., Wang, D., … Mucke, L. (2014). Life Extension Factor Klotho Enhances Cognition. *Cell Reports*, *7*(4), 1065–1076.

Dubal, D. B., Zhu, L., Sanchez, P. E., Worden, K., Broestl, L., Johnson, E., … Mucke, L. (2015). Life Extension Factor Klotho Prevents Mortality and Enhances Cognition in hAPP Transgenic Mice. *The Journal of Neuroscience*, *35*(6), 2358–2371.

Farrow, E. G., Imel, E. A., & White, K. E. (2011). Hyperphosphatemic familial tumoral calcinosis

(FGF23, GALNT3 and α-Klotho). *Best Practice & Research. Clinical Rheumatology*, *25*(5), 735–47.

Hardy, J. (2009, August). The amyloid hypothesis for Alzheimer's disease: A critical reappraisal. *Journal of Neurochemistry, 110* (4), 1129-1134.

Herrup, K. (2010). Re-imaging Alzheimer's disease - an age-based hypothesis. *Journal of Neuroscience*, *30*(50), 16755–16762.

Hu, M. C., Kuro-o, M., & Moe, O. W. (2012). Secreted klotho and chronic kidney disease. *Advances in Experimental Medicine and Biology*, *728*, 126–57.

Kim, J.-H., Hwang, K.-H., Park, K.-S., Kong, I. D., & Cha, S.-K. (2015). Biological Role of Anti-aging Protein Klotho. *Journal of Lifestyle Medicine*, *5*(1), 1–6.

Köpke, E., Tung, Y. C., Shaikh, S., Alonso, A. D. C., Iqbal, K., & Grundke-Iqbal, I. (1993). Microtubule-associated protein tau. Abnormal phosphorylation of a non-paired helical filament pool in Alzheimer disease. *Journal of Biological Chemistry*, *268*(32), 24374–24384.

Kosakai, A., Ito, D., Nihei, Y., Yamashita, S., Okada, Y., Takahashi, K., & Suzuki, N. (2011). Degeneration of mesencephalic dopaminergic neurons in klotho mouse related to vitamin D exposure. *Brain Research*, *1382*, 109–117.

Kuang, X., Chen, Y. S., Wang, L. F., Li, Y. J., Liu, K., Zhang, M. X., … Du, J. R. (2014). Klotho upregulation contributes to the neuroprotection of ligustilide in an alzheimer's disease mouse model. *Neurobiology of Aging*, *35*(1), 169–178.

Kumar, A., & Dogra, S. (2008). Neuropathology and therapeutic management of Alzheimer's disease - An update. *Drugs of the Future*, *33*(5), 433–446.

Kumar, A., Singh, A., & Ekavali. (2015). A review on Alzheimer's disease pathophysiology and its management: An update. *Pharmacological Reports*, *67*(2), 195–203.

Kuro-o, M. (2006). Klotho as a regulator of fibroblast growth factor signaling and phosphate/calcium metabolism. *Current Opinion in Nephrology and Hypertension*, *15*(4), 437–441.

Kuro-O, M. (2010). Klotho. *Pflugers Archiv European Journal of Physiology*, *459*(2), 333-343.

Kuro-o, M., Matsumura, Y., Aizawa, H., Kawaguchi, H., Suga, T., Utsugi, T., … Nabeshima, Y. I. (1997). Mutation of the mouse klotho gene leads to a syndrome resembling ageing. *Nature*, *390*(6655), 45–51.

Kurosu, H., Yamamoto, M., Clark, J. D., Pastor, J. V, Nandi, A., Gurnani, P., … Kuro-o, M. (2005). Suppression of aging in mice by the hormone Klotho. *Science*, *309*(5742), 1829–33.

Kusaba, T., Okigaki, M., Matui, A., Murakami, M., Ishikawa, K., Kimura, T., … Matsubara, H. (2010). Klotho is associated with VEGF receptor-2 and the transient receptor potential canonical-1 Ca2+ channel to maintain endothelial integrity. *Proceedings of the National Academy of Sciences of the United States of America*, *107*(45), 19308–13.

Lee, G., Neve, R. L., & Kosik, K. S. (1989). The microtubule binding domain of tau protein. *Neuron*, *2*(6), 1615–1624.

Lewczuk, P., Mroczko, B., Fagan, A., & Kornhuber, J. (2015). Biomarkers of Alzheimer's disease and mild cognitive impairment: A current perspective. *Advances in Medical Sciences*, *60*(1), 76-82.

Li, S.-A., Watanabe, M., Yamada, H., Nagai, A., Kinuta, M., & Takei, K. (2004). Immunohistochemical localization of Klotho protein in brain, kidney, and reproductive

organs of mice. *Cell Structure and Function*, *29*(4), 91–99.

Lin, Y., & Sun, Z. (2012). Antiaging gene Klotho enhances glucose-induced insulin secretion by up-regulating plasma membrane levels of TRPV2 in MIN6 beta-cells. *Endocrinology*, *153*(7), 3029–3039.

Liu, H., Fergusson, M. M., Castilho, R. M., Liu, J., Cao, L., Chen, J., … Finkel, T. (2007). Augmented Wnt signaling in a mammalian model of accelerated aging. *Science*, *317*(5839), 803–806.

Massó, A., Sánchez, A., Gimenez-Llort, L., Lizcano, J. M., Cañete, M., Garciá, B., … Chillon, M. (2015). Secreted and transmembrane αklotho isoforms have different spatio-temporal profiles in the brain during aging and Alzheimer's disease progression. *PLoS ONE*, *10*(11), 1–15.

Matsumura, Y., Aizawa, H., Takako, S.-I., Nagai, R., Kuro-o, M., & Nabeshima, Y. (1998). Identification of the Human Klotho Gene and Its Two Transcripts Encoding Membrane and Secreted Klotho Protein1. *Biochemical and Biophysical Research Communications*, *242*(1–2), 626–630.

Mazanetz, M. P., & Fischer, P. M. (2007). Untangling tau hyperphosphorylation in drug design for neurodegenerative diseases. *Nature Reviews. Drug Discovery*, *6*(6), 464–79.

Mori, K., Yahata, K., Mukoyama, M., Suganami, T., Makino, H., Nagae, T., … Nakao, K. (2000). Disruption of klotho gene causes an abnormal energy homeostasis in mice. *Biochemical and Biophysical Research Communications*, *278*(3), 665–70.

Müller, U. C., & Zheng, H. (2012). Physiological functions of APP family proteins. *Cold Spring Harbor Perspectives in Medicine*, *2*(2), a006288.

Muresan, V., & Ladescu Muresan, Z. (2015). Amyloid-β precursor protein: Multiple fragments, numerous transport routes and mechanisms. *Experimental Cell Research*, *334*(1), 45–53.

Nagai, T., Yamada, K., Kim, H.-C., Kim, Y.-S., Noda, Y., Imura, A., … Nabeshima, T. (2003). Cognition impairment in the genetic model of aging klotho gene mutant mice: a role of oxidative stress. *The FASEB Journal*, *17*(1), 50–2.

Nhan, H. S., Chiang, K., & Koo, E. H. (2015). The multifaceted nature of amyloid precursor protein and its proteolytic fragments: friends and foes. *Acta Neuropathologica*, *129*(1), 1-19.

Nunan, J., & Small, D. H. (2000). Regulation of APP cleavage by alpha-, beta- and gamma-secretases. *FEBS Letters*,*483*(1), 6-10.

Olauson, H., Lindberg, K., Amin, R., Jia, T., Wernerson, A., Andersson, G., & Larsson, T. E. (2012). Targeted Deletion of Klotho in Kidney Distal Tubule Disrupts Mineral Metabolism. *Journal of the American Society of Nephrology*, *23*(10), 1641–1651.

Ross, C. A., & Poirier, M. A. (2004). Protein aggregation and neurodegenerative disease. *Nature Medicine*, *10 Suppl*(July), S10-7.

Roth, A. D., Ramírez, G., Alarcón, R., & Von Bernhardi, R. (2005). Oligodendrocytes damage in Alzheimer's disease: Beta amyloid toxicity and inflammation. *Biological Research*, *38*(4), 381–387.

Roy, S., Zhang, B., Lee, V. M. Y., & Trojanowski, J. Q. (2005). Axonal transport defects: A common theme in neurodegenerative diseases. *Acta Neuropathologica*, *109*(1), 5-13.

Salomone, S., Caraci, F., Leggio, G. M., Fedotova, J., & Drago, F. (2012). New pharmacological strategies for treatment of Alzheimer's disease: Focus on disease modifying drugs. *British Journal of Clinical Pharmacology*, *73*(4), 504–517.

Satoh, M., Nagasu, H., Morita, Y., Yamaguchi, T. P., Kanwar, Y. S., & Kashihara, N. (2012). Klotho protects against mouse renal fibrosis by inhibiting Wnt signaling. *AJP: Renal Physiology*, *303*(26), 1641–1651.

Semba, R. D., Moghekar, A. R., Hu, J., Sun, K., Turner, R., Ferrucci, L., & O'Brien, R. (2014). Klotho in the cerebrospinal fluid of adults with and without Alzheimer's disease. *Neuroscience Letters*, *558*, 37–40.

Sena, L. A., & Chandel, N. S. (2012). Physiological roles of mitochondrial reactive oxygen species. *Molecular Cell*, *48*(2), 158-166.

Shiozaki, M., Yoshimura, K., Shibata, M., Koike, M., Matsuura, N., Uchiyama, Y., & Gotow, T. (2008). Morphological and biochemical signs of age-related neurodegenerative changes in klotho mutant mice. *Neuroscience*, *152*(4), 924–941.

Shiraki-Iida, T., Aizawa, H., Matsumura, Y., Sekine, S., Iida, A., Anazawa, H., … Nabeshima, Y. I. (1998). Structure of the mouse klotho gene and its two transcripts encoding membrane and secreted protein. *FEBS Letters*, *424*(1–2), 6–10.

Sonawane, N. D., Szoka, F. C., & Verkman, A. S. (2003). Chloride Accumulation and Swelling in Endosomes Enhances DNA Transfer by Polyamine-DNA Polyplexes. *Journal of Biological Chemistry*, *278*(45), 44826–44831.

Tanaka, Y., & Deluca, H. F. (1974). Role of 1,25-dihydroxyvitamin D3 in maintaining serum phosphorus and curing rickets. *Proceedings of the National Academy of Sciences of the United States of America*, *71*(4), 1040–1044.

Tanzi, R. E., & Bertram, L. (2005). Twenty years of the Alzheimer's disease amyloid hypothesis: A genetic perspective. *Cell*, *120*(4), 545–555.

Tucker, R. P. (1990). The roles of microtubule-associated proteins in brain morphogenesis: a review. *Brain Research Reviews*, *15*(2), 101-120.

Uchida, A., Komiya, Y., Tashiro, T., Yorifuji, H., Kishimoto, T., Nabeshima, Y., & Hisanaga, S. I. (2001). Neurofilaments of Klotho, the mutant mouse prematurely displaying symptoms resembling human aging. *Journal of Neuroscience Research*, *64*(4), 364–370.

Urakawa, I., Yamazaki, Y., Shimada, T., Iijima, K., Hasegawa, H., Okawa, K., … Yamashita, T. (2006). Klotho converts canonical FGF receptor into a specific receptor for FGF23. *Nature*, *444*(7120), 770–774.

Utsugi, T., Ohno, T., Ohyama, Y., Uchiyama, T., Saito, Y., Matsumura, Y., … Nagai, R. (2000). Decreased insulin production and increased insulin sensitivity in the klotho mutant mouse, a novel animal model for human aging. *Metabolism: Clinical and Experimental*, *49*(9), 1118–1123.

Wang, Y., Kuro-O, M., & Sun, Z. (2012). Klotho gene delivery suppresses Nox2 expression and attenuates oxidative stress in rat aortic smooth muscle cells via the cAMP-PKA pathway. *Aging Cell*, *11*(3), 410–417.

Wang, Y., & Sun, Z. (2009). Current understanding of klotho. *Ageing Research Reviews*, *8*(1), 43-51.

Xu, Y., & Sun, Z. (2015). Molecular basis of klotho: From gene to function in aging. *Endocrine Reviews*, *36*(2), 174–193.

Yamamoto, M., Clark, J. D., Pastor, J. V, Gurnani, P., Nandi, A., Kurosu, H., … Kuro-o, M. (2005). Regulation of oxidative stress by the anti-aging hormone klotho. *The Journal of Biological Chemistry*, *280*(45), 38029–34.

Zeldich, E., Chen, C.-D. Di, Colvin, T. A., Bove-Fenderson, E. A., Liang, J., Tucker Zhou, T. B.,

… Abraham, C. R. (2014). The neuroprotective effect of Klotho is mediated via regulation of members of the redox system. *Journal of Biological Chemistry*, *289*(35), 24700–24715.